Journal of Molecular Structure 1330 (2025) 141347

Contents lists available at ScienceDirect

Journal of Molecular Structure

journal homepage: www.elsevier.com/locate/molstr

Structural and computational insights into a benzene sulfonamide derivative: Hirshfeld surface, energy framework, optical, NBO, electronic and biological properties

N. Kanagathara [a], G. Dhanalakshmi [b], E. Mohanapriya [a], Palani Manikandan [c], A.K. Mohanakrishnan [c], V. Sabari [d], Dabora Vincy [d], V. Ragavendran [e], S. Aravindhan [f,*]

[a] Department of Physics, Saveetha School of Engineering, Saveetha Institute of Medical and Technical Sciences, Saveetha University, Thandalam, Chennai 602 105, India
[b] Department of Physics, Mannar Thirumalai Naicker College (Autonomous), Madurai, Tamilnadu, India
[c] Department of Organic Chemistry, University of Madras, Guindy Campus, Chennai, India
[d] Department of Physics, Marudhar Kesari Jain College for Women, Vaniyampadi 635 751, Tamilnadu, India
[e] Department of Physics, Rajalakshmi Engineering College, Thandalam, Chennai 602 105, India
[f] PG & Research Department of Physics, Presidency College (Autonomous), Chennai, India

ARTICLE INFO

Keywords:
Benzenesulfonamide
Hirshfeld surface analysis
Molecular Electrostatic Potential (MEP)
Molecular docking

ABSTRACT

The benzene sulfonamides (BS) derivative, with the chemical formula $C_{31}H_{23}ClN_2O_4S_2$, is an organic compound that crystallizes in the triclinic system with the space group P-1. The lattice parameters are determined as follows: a=9.1558(5) Å, b=9.9077(5) Å, c=16.1367(8) Å, α =91.329(3)°; β=98.192(3)°; γ = 101.108(3)°, and the unit cell volume V=1419.79(13) (Å)^3. Furthermore, comprehensive theoretical studies have been conducted using the B3PW91/6-31g(d,p) basis set to gain deeper insights into the molecular structure, vibrational characteristics, and bonding interactions of the compound. This computational approach enables a detailed analysis of the electronic properties and the underlying forces that govern the stability and reactivity of the molecule. Hirshfeld surface analysis and two-dimensional fingerprint plots to investigate the interactions between the crystal's constituent units and the factors influencing its structural arrangement. Molecular electrostatic potential (MEP) analysis has been performed to visualize the charge distribution within the molecule, identifying regions of electron density and potential reactive sites, thereby providing insight into the compound's intermolecular interactions and chemical reactivity. Energy frameworks visualize how forces like hydrogen bonds and van der Waals interactions shape the stability and structure of molecular crystals. Natural Bonding Orbital (NBO) analysis of the BS derivative reveals key insights into its electronic structure and bonding interactions. The Energy gap (HOMO-LUMO) highlights the compound's stability and reactivity, and UV-Visible spectroscopy confirms these findings by showcasing its electronic transitions and absorption properties. Together, these techniques provide a detailed understanding of the BS derivative's electronic behavior. Electron Localization Function (ELF) provides insight into the spatial distribution of electron pairs, indicating regions of localization and delocalization. Meanwhile, Localized Orbital Locator (LOL) quantifies the contribution of localized orbitals to the electron density, offering a detailed understanding of bonding interactions and electronic properties within the BS derivative compound. The Fukui function (FF) reveals the reactivity of molecular systems by identifying regions of electron density that are most likely goes to nucleophilic or electrophilic attacks. Moreover, molecular docking analysis have performed to evaluate the potential of the benzene sulfonamide (BS) derivative as a drug candidate.

1. Introduction

The BS derivative, with the chemical formula $C_{31}H_{23}ClN_2O_4S_2$, is an organic compound that crystallizes in the triclinic system. It consists of a benzene ring attached to a sulfonamide group (-SO_2NH_2). It belongs to the P-1 space group, which exhibits minimal symmetry and has no

* Corresponding author.
E-mail address: aravindhanpresidency@gmail.com (S. Aravindhan).

https://doi.org/10.1016/j.molstruc.2025.141347
Received 8 October 2024; Received in revised form 28 December 2024; Accepted 5 January 2025
Available online 12 January 2025

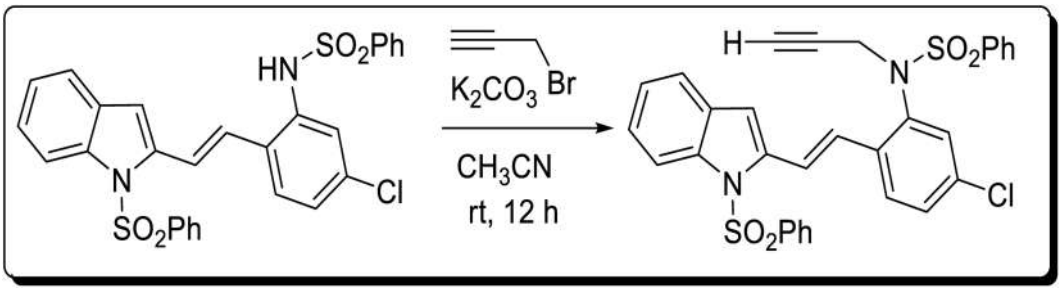

Scheme 1. Synthetic way of the BS Derivative.

specific metric restrictions on the unit cell parameters. Sulfonamide is a type of synthetic drug used to treat various bacterial infections in humans and animals. It was the first effective antibacterial agent and paved the way for modern antibiotics [1]. The SO_3NH group in sulfonamides is responsible for their antibacterial properties. However, sulfonamides are not easily broken down in the environment and can cause various side effects, such as digestive and respiratory issues [2]. Some non-allergic reactions to sulfonamides include diarrhea, nausea, vomiting, dizziness, candidiasis, folate deficiency, and headaches [3]. BSs and their derivatives are known for their impressive range of properties including antibacterial [4–5], anti-tumour, insulin-stimulating, and anti-thyroid effects. BSs, also known as "sulfa pills", are a crucial class of drugs in organic chemistry [6]. The sulfonamide group is widely used in modern medicine, playing a crucial role in treating bacterial infections and showing potential for treating fungal infections [7]. Sulfonamide derivatives are highly favored in medicinal chemistry due to their broad range of pharmacological activities [8–10]. and tuberculosis [11–12]. Sulfonamide and its derivatives have synthetic and therapeutic applications [13–14]. It has extensively studied the synthesis and pharmacological properties of sulfonamide-containing compounds, which are important for drug development [15]. These compounds are effective in treating various conditions, including vascular diseases, post-surgical pain, cancer pain, and several types of arthritis.

In addition to their medicinal applications, benzene sulfonamides (BS) are widely used as intermediates in the synthesis of organic compounds, including dyes, pigments, and other specialty chemicals. This versatility highlights their importance in both medicine and industrial chemistry [17]. The synthesis and study of substituted benzene sulfonamides, including their structures and properties, is an important research area due to their wide biological importance. The structure of benzenesulfonamide was reported by Gowda et al. in the year 2007 and identified the structure belong to monoclinic system with space group P*c* [16]. These compounds have diverse biological activities and are extensively explored for their therapeutic potential. Literature review on Schiff bases derived from BS [1], BS derivatives incorporated into the triazine ring [17], 4-[(2-hydroxy-3-methylbenzylidene) amino]BS [18], (E)-4-((2-hydroxy-3,5-diiodobenzylidene) amino)-N-(pyrimidine)-2-yl) BS [19], benzene sulfonamide-derived Schiff base copper (II) [20], N-(5-acetyl-4-methylpyrimidin-2-yl) BS are reported [21]. In this study, a BS derivative was synthesized and its vibrational characteristics were analyzed. Hirshfeld analysis, Energy Framework analysis, NBO analysis, HOMO-LUMO energy gap calculations, UV-Visible studies, and biological evaluations were performed to gain insights into the molecular properties, electronic structure, and intermolecular interactions of the compound. These techniques have significantly advanced our understanding of chemical structures and played a key role in the development of new materials, pharmaceuticals, and chemical applications.

Table 1
Crystal data and refinement parameters for BS derivative compound.

Empirical formula	$C_{31}\ H_{23}Cl\ N_2\ O_4\ S_2$
Formula weight	587.08
Temperature	296(2) K
Wavelength	0.71073 Å
Crystal system	Triclinic
Space group	P -1
Unit cell dimensions	a = 9.1558(5) Å; α = 91.329(3)° b = 9.9077(5) Å; β= 98.192(3)° c=16.1367(8)Å; γ = 101.108(3)°
Volume	1419.79(13)Å^3
Z	2
Density (calculated)	1.373 Mg/m^3
Absorption coefficient	0.321 mm^{-1}
F (000)	608
Crystal size	0.250×0.200×0.200 mm^3
Theta range for data collection	2.098 to 28.661 deg.
Index ranges	-12≤h≤12, -13≤k≤13, -21≤l≤21
Reflections collected	33874
Independent reflections	7268 [R(int) = 0.0592]
Completeness to theta = 25.242°	100.00 %
Absorption correction	Semi-empirical from equivalents
Max. and min. transmission	0.7457 and 0.6168
Refinement method	Full-matrix least-squares on F^2
Data / restraints / parameters	7268 / 0 / 374
Goodness-of-fit on F2	1.011
Final R indices [I>2sigma(I)]	R1 = 0.0463,wR2=0.0991
R indices (all data)	R1 = 0.1017,wR2=0.1239
Largest diff. peak and hole	0.259 and -0.343 e.A^{-3}

2. Experimental

2.1. Materials and methods

To a solution of (E)-N-(5-chloro-2-(2-(1-(phenylsulfonyl)-1H-indol-2-yl) vinyl) phenyl) BS (0.3 g, 0.530 mmol) in CH_3CN (10 mL) was combined with K_2CO_3 (0.14 g, 1.060 mmol) and propargyl bromide (0.096 mL, 1.060 mmol). The mixture was stirred at room temperature for 12 h, as illustrated in Scheme 1.

After the reaction was completed (as monitored by TLC), the mixture was poured onto crushed ice (50 g) containing concentrated HCl (5 mL). It was then extracted with ethyl acetate (2 × 20 mL), washed with water (2 × 20 mL), and dried over Na_2SO_4. The solvent was removed under reduced pressure, and the resulting residue was crystallized from methanol (4 mL) to yield BS as a white solid.

^{1}H NMR (300 MHz, $CDCl_3$): δ 8.23 (d, J = 8.1 Hz, 1 H), 7.85-7.76 (m, 6 H), 7.67-7.62 (m, 1 H), 7.56-7.44 (m, 5 H), 7.42-7.29 (m, 4 H), 7.26-7.24 (m, 1 H), 6.88 (d, J = 1.8 Hz, 1 H), 6.18 (s, 1 H), 4.42 (s, 2 H), 2.20 (t, J = 2.4 Hz, 1 H) ppm; ^{13}C NMR (75 MHz, $CDCl_3$): δ139.5, 138.8, 138.3, 137.7, 136.8, 133.7, 133.6, 133.4, 130.2, 129.8, 129.1, 129.0, 128.1, 127.8, 126.8, 126.7, 125.1, 124.3, 121.6, 120.9, 115.4, 110.1, 74.5, 41.7 ppm.

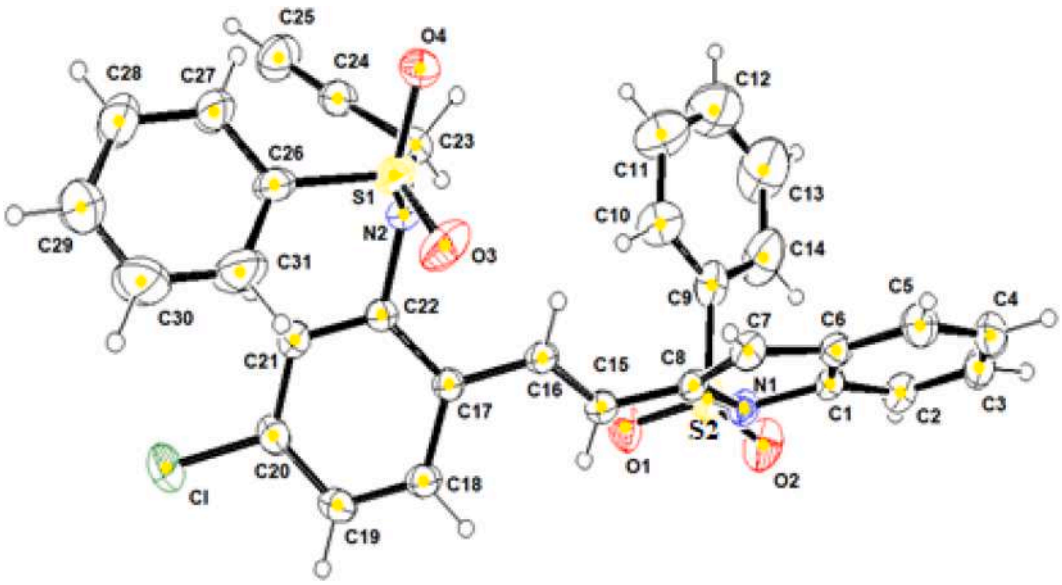

Fig. 1. ORTEP plot of BS derivative with the atom numbering scheme. Displacement ellipsoids are drawn at 40 % probability level.

2.2. X-ray single crystal data collection

The X-ray intensity data for selected single crystal of BS was recorded on a four -circle κ geometry Xcalibur diffractometer with Sapphire2 area CCD detector, at room temperature. Data collections were made using the CrysAlis CCD program [22]. The structures were solved by the direct methods using SHELXT-2014/7 [23] and refined using SHELXL-2018/3 program [24]. MERCURY and ORTEP-PLATON [25] were used to construct the figures [26–28]. The hydrogen atoms were treated as riding on their parent atoms. The data collection parameters, crystallographic data, and final agreement parameters are summarized in Table 1.

2.3. Computational characterization

Molecular orbital calculations, including full geometry optimization of the hydrogen-bonded Benzenesulfanoamide, were performed using the Gaussian16 program package [29]. All computations employed the density functional theory (DFT) method with the B3PW91 functional, utilizing the 6-31G (d,p) basis set [30]. The initial geometries were derived from the structures obtained through X-ray diffraction analysis. The Electron Localization Function (ELF) and Localized Orbital Locator (LOL) were calculated and visualized using Multiwfn 3.8 software [31]. The Hirshfeld surface analysis and the 2D fingerprint plots were performed using the Crystal Explorer program package, version 3.1 [32]. The crystal structure was imported using CIF (Crystallographic Information File) files. Hirshfeld surfaces were then constructed for both the complete complex molecule and its individual building blocks at an exceptionally high resolution. These surfaces were mapped using the d_{norm} function to highlight regions of close intermolecular contacts. Furthermore, 2D fingerprint plots were performed with the same software, providing a visual and quantitative representation of the various intermolecular interactions contributing to the crystal packing.

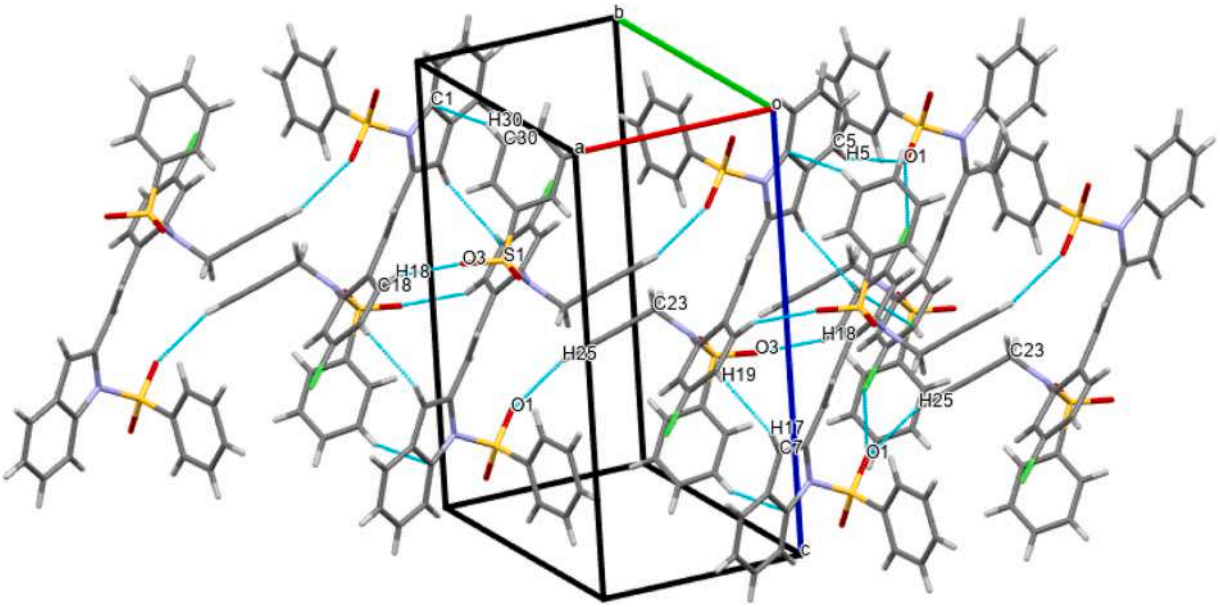

Fig. 2. Packing diagram of BS derivative.

Table 2
Hydrogen bond interactions for BS [Å and °].

D-H…A	d(D-H)	d(H…A)	d(D…A)	<(DHA)
C(2)-H(2)…O(2)	0.93	2.42	2.994(3)	120.2
C5-H5…O1	0.93	2.52	3.3729(2	152
C18-H18 …O3	0.93	2.54	3.4096(2)	157
C25-H25…O1	0.93	2.52	3.4200(2)	164
C30-H30...π	0.93	2.99	3.7788(2)	144

3. Results and Discussion

3.1. Structural characterization

The crystalline structure of BS forms in the space group P-1 within the triclinic system, with two molecules in each unit cell. Table 1 provides the crystal data and additional structural information related to BS. The molecular structure and packing diagram are presented in Figs. 1 and 2 respectively. The BS rings form a dihedral angle of 87.33 (10)° with the indole ring system, indicating an equatorial orientation. The corresponding DFT computed value is 85.9741°. The torsion angle for atoms C14-C9-S2-N1 is 113.0(3)°, suggesting a (+) anti-clinal relationship with the indole ring, while the torsion angle for atoms C8-C15-C16-C17 is -178.0(2)°, indicating a (-) anti-periplanar orientation relative to the chlorophenyl ring. The corresponding DFT counterpart is -174.79°. The torsion angle for atoms C31-C26-S1-N2 is 97.3(3)°, showing a (+) anticlinal orientation with respect to the BS ring experimentally and theoretically this value is computed at 98.597°. The chlorine atom (Cl) attached to the C20 position of the phenyl ring is equatorial, as confirmed by the torsion angle value of C18-C19-C20-Cl experimentally at 179.79(18)° and theoretically at 179.85°. The bond angles for atoms O3-S1-O4 and O2-S2-O1 are 119.60(12)° and 119.75 (11)°, respectively. The corresponding bond angles are 122.15° and 121.20°. The total bond angles around N_2 in the title compound amount to 367.34°, suggesting sp^2 hybridization [33]. Table 2 presented the hydrogen bond symmetry parameters of BS derivative. Table 3 presents the optimized geometric parameters of the BS derivative along with calculated using the DFT method with the B3PW91/6-31g(d,p) basis set. Fig. 3 shows the optimized structure as a result of these DFT calculations. The BS molecular structure comprises two BS rings, one benzimidazolium ring, and one phenyl ring with a chlorine atom attached. In the BS compound, the SO_2 groups are bonded to both the phenyl and benzimidazolium rings.

In the BS crystal, the molecules are linked via C5—H5…O1, C18—H18…O3, C25— H25…O1, C30— H30…π hydrogen bonds forming C(8) chains that propagate along the c-axis direction, as shown in Fig. 2 (two-dimensional network). The C1—N52 and C13—S59 Å bond lengths of 1.4117 and 1.783 Å, respectively, are in the ranges of normal C S and C N bond lengths, indicating double-bond character and thus confirming the keto tautomeric form and are comparable with those in related structures. The corresponding computed bond distance are 1.4117 Å and 1.783 Å. The bond parameters of the present BS derivative are almost similar to the other BS derivatives except for little bit difference in the S—O bond length. Pure benzenesulfonamide may have the bond length of 1.408 Å whereas the present BS derivative has 1.424 Å [34–35]. The increase in bond length of 0.016 Å reflects the reduced electron density and this variation alter the molecular polarity as well as hydrogen bonding potential. The other BS derivatives has S—O bond length of (E)-4-((2-hydroxy-3,5-diiodobenzylidene)amino)--N-(pyrimidine)-2-yl)benzenesulfonamide,

N-(5-acetyl-4-methylpyrimidin-2-yl)benzenesulfonamide, N-(4-Chlorophenyl)-2-nitrobenzenesulfonamide, 4,6-Dimethylbenzene-1,3-disulfonamide 1.420 Å, 1.423 Å, 1.425 Å, 1.436 Å, respectively. The bond lengths, bond angles, agree very well with literature values [19,21, 36–37].

Table 3
Geometrical parameters of BS derivative compound.

ATOM	Bond Length (Å)		ATOM	Bond Angle (°)	
	Theoretical	Experimental		Theoretical	Experimental
C1-C2	1.3964	1.382	C2-C1-C10	121.5332	122.12
C1-C10	1.4154	1.398	C2-C1-N52	131.1898	130.65
C1-N52	1.4117	1.427	C10-C1-N52	107.2248	107.11
C2-H3	1.0819	0.930	C1-C2-H3	121.3324	121.44
C2-C4	1.3911	1.383	C1-C2-C4	117.4186	117.09
C4-H5	1.0862	0.930	H3-C2-C4	121.2417	121.47
C4-C6	1.4041	1.377	C2-C4-H5	118.7785	119.13
C6-H7	1.0861	0.930	C2-C4-C6	121.782	121.73
C6-C8	1.3858	1.377	H5-C4-C6	119.4326	119.14
C8-H9	1.0861	0.930	C4-C6-H7	119.5174	119.49
C8-C10	1.4024	1.397	C4-C6-C8	120.6309	212.02
C10-C11	1.4275	1.425	H7-C6-C8	119.8489	119.14
			C6-C8-H9	121.0355	120.46
C11-C12	1.3705	1.349	C6-C8-C10	118.8193	121.02
C11-H63	1.0816	0.947	H9-C8-C10	120.1452	120.42
C12-C24	1.4484	1.450	C1-C10-C8	119.8031	118.90
C12-N52	1.4238	1.435	C1-C10-C11	107.5286	107.68
C13-C14	1.394	1.377	C8-C10-C11	132.6483	133.39
C13-C22	1.3953	1.370	C10-C11-C12	108.8273	109.84
C13-S59	1.783	1.743	C10-C11-H63	126.6124	126.27
C14-H15	1.0843	0.930	C12-C11-H63	124.3814	123.83
C14-C16	1.3927	1.375	C11-C12-C24	127.9159	120.50
C16-H17	1.0859	0.930	C11-C12-N52	108.1884	107.83
C16-C18	1.3943	1.359	C24-C12-N52	123.7609	122.28
C18-H19	1.0861	0.930	C14-C13-C22	121.8706	120.89
C18-C20	1.395	1.374	C14-C13-S59	119.0706	119.42
C20-H21	1.0857	0.930	C22-C13-S59	119.0588	119.68
C20-C22	1.3917	1.382	C13-C14-H15	119.8046	120.77
C22-H23	1.0845	0.930	C13-C14-C16	118.7025	118.55
C24-C25	1.3509	1.331	H15-C14-C16	121.4875	120.68

(continued on next page)

Table 3 (*continued*)

ATOM	Bond Length (Å)		ATOM	Bond Angle (°)	
	Theoretical	Experimental		Theoretical	Experimental
C24-H62	1.0843	0.956	C14-C16-H17	119.6685	119.84
C25-C26	1.4579	1.462	C14-C16-C18	120.1587	120.41
C25-H61	1.085	0.923	H17-C16-C18	120.1715	119.75
C26-C27	1.4061	1.401	C16-C18-H19	119.8187	119.60
C26-C34	1.4147	1.400	C16-C18-C20	120.402	120.68
C27-H28	1.0852	0.930	H19-C18-C20	119.778	119.72
C27-C29	1.387	1.373	C18-C20-H21	120.1921	120.23
C29-H30	1.0847	0.930	C18-C20-C22	120.1618	119.53
C29-C31	1.3936	1.375	H21-C20-C22	119.6446	120.24
C31-C32	1.3898	1.379	C13-C22-C20	118.7015	119.94
C31-Cl60	1.7442	1.736	C13-C22-H23	120.2023	119.99
C32-H33	1.0832	0.930	C20-C22-H23	121.0927	120.08
C32-C34	1.3964	1.385	C12-C24-C25	122.2996	124.72
C34-N53	1.4315	1.445	C12-C24-H62	116.7385	115.26
C35-H36	1.0941	0.970	C25-C24-H62	120.9599	120.01
C35-H37	1.0965	0.970	C24-C25-C26	125.4365	122.82
C35-C38	1.4654	1.463	C24-C25-H61	119.1388	119.61
C35-N53	1.466	1.467	C26-C25-H61	115.4219	117.49
C38-C39	1.2086	1.167	C25-C26-C27	122.4151	120.73
C39-H40	1.0667	0.930	C25-C26-C34	120.4434	122.24
C41-C42	1.395	1.370	C27-C26-C34	117.1409	116.95
C41-C50	1.3948	1.363	C26-C27-H28	119.2149	119.15
C41-S58	1.7867	1.764	C26-C27-C29	122.151	121.70
C42-H43	1.0845	0.930	H28-C27-C29	118.6205	119.15
C42-C44	1.392	1.380	C27-C29-H30	120.6363	120.16
			C27-C29-C31	119.2388	119.71
C44-H45	1.0859	0.930	H30-C29-C31	120.121	120.13
C44-C46	1.3951	1.347	C29-C31-C32	120.6444	120.75
C46-H47	1.0862	0.929	C29-C31-Cl60	119.7773	119.13
C46-C48	1.3943	1.363	C32-C31-Cl60	119.5776	120.10
C48-H49	1.0858	0.930	C31-C32-H33	120.6163	120.40
C48-C50	1.3928	1.375	C31-C32-C34	119.6457	119.24
C50-H51	1.0846	0.930	H33-C32-C34	119.7308	120.37
N52-S59	1.7159	1.665	C26-C34-C32	121.1732	121.53
N53-S58	1.6868	1.632	C26-C34-N53	119.6028	119.29
O54-S59	1.4562	1.424	C32-C34-N53	119.1696	119.18
			H36-C35-H37	107.0435	107.43
O55-S59	1.4549	1.423	H36-C35-C38	110.03	108.33
O56-S58	1.4587	1.429	H36-C35-N53	107.1399	108.34
O57-S58	1.462	1.425	H37-C35-C38	109.6427	108.31
			H37-C35-N53	106.8905	108.32
			C38-C35-N53	115.709	115.83
			C42-C41-C50	121.6414	119.43
			C42-C41-S58	119.2993	119.82
			C50-C41-S58	119.0594	119.43
			C41-C42-H43	119.9859	119.83
			C41-C42-C44	118.8409	119.78
			C43-C42-C44	121.1652	120.39

(*continued on next page*)

Table 3 (*continued*)

ATOM	Bond Length (Å)		ATOM	Bond Angle (°)	
	Theoretical	Experimental		Theoretical	Experimental
			C42-C44-H45	119.6721	120.03
			C42-C44-C46	120.1658	120.05
			H45-C44-C46	120.1605	119.92
			C44-C46-H47	119.8192	120.15
			C44-C46-C48	120.3554	119.68
			H47-C46-C48	119.8237	120.17
			C46-C48-H49	120.2033	119.92
			C46-C48-C50	120.1267	120.05
			H49-C48-C50	119.6692	120.03
			C41-C50-C48	118.867	119.46
			C41-C50-H51	119.6683	120.27
			C48-C50-H51	121.4558	120.27
			C1-N52-C12	108.1874	107.47
			C1-N52-S59	122.7457	120.13
			C34-N53-C35	123.4208	119.50
			C34-N53-S58	119.0688	118.14
			C35-N53-S58	119.4644	121.24
			C41-S58-N53	108.1544	106.68
			C41-S58-O56	107.0869	107.10
			C41-S58-O57	107.7005	109.21
			N53-S58-O56	105.8592	107.75
			N53-S58-O57	105.2482	105.84
			O56-S58-O57	122.152	119.60
			C13-S59-N52	104.5493	105.09
			C13-S59-O54	108.4228	108.81
			C13-S59-O55	108.7455	108.80
			N52-S59-O54	106.7316	106.86
			N52-S59-O55	105.9509	106.59
			O54-S59-O55	121.2	119.72

3.2. Hirshfeld surface analysis

Hirshfeld surface analysis (HS) [38] and 2D fingerprint plots [39] have become powerful tool for the detailed examination of crystal structures, allowing for both qualitative and quantitative assessments. These techniques involve the calculation and visualization of surfaces that represent the regions around a molecule where intermolecular interactions occur. By applying specific functions like d_{norm} (normalized contact distance), shape index, and curvature, the analysis provides a parameterization of these surfaces at each point within the crystal network. This process yields essential insights into the nature and strength of interactions between molecules, such as hydrogen bonds, van der Waals forces, and π-π stacking. For studying hydrogen-bonded systems, mapping with the d_{norm} function is particularly effective. The d_{norm} function uses a color-coding scheme where red areas indicate strong hydrogen bonding interactions. These red regions appear when the sum of the distances from the Hirshfeld surface to the nearest internal (d_i) and external (d_e) atoms is significantly shorter than the sum of the van der Waals radii of the interacting atoms. The shape index provides information on the contours of the electron density surface surrounding the molecular interactions.

The Hirshfeld surface of the studied compound was mapped over various properties, including d_{norm}, electrostatic potential, shape index, curvedness, and fragment patches (Fig. 4). A small red spot on the Hirshfeld surface mapped onto d_{norm} Fig. 4(a) represents the presence of a C-H…O interaction. The red and blue triangles visible on the Hirshfeld surface projected onto the shape-indexed surfaces Fig. 4(b), as well as the flat regions on the curvedness surface Fig. 4(c), indicate the presence of specific interactions. The red and blue regions on the Hirshfeld surface overlaid with the electrostatic potential illustrate regions of negative potential around the acceptor atoms and positive potential around the donor atoms, respectively. The coloured patches on the Hirshfeld surface are used to determine the coordination environment of the molecule's nearest neighbours, which was found to be 12 in Fig. 4(e). Two-dimensional fingerprint plots of the compound's Hirshfeld surface are shown in Fig. 5, highlighting the various contacts, including H…H, C…H/H…C, O…C/C…O, and C…C. These contacts are characterized by distinctive pseudosymmetry wings located on the upper left and lower right sides of the diagonal axis representing d_e and d_i. The largest region on the fingerprint plot corresponds to H…H interactions, which are densely concentrated in the central area at $d_e = d_i \approx 1.2$ Å, contributing 35.5 % to the overall Hirshfeld surface. The C…H/H…C interactions, with nearly the same $d_e + d_i \approx 2.7$ Å and contributing 28.3 % to the Hirshfeld surface, form the next largest region and are concentrated along the edges. The C…O/O…C interactions, contributing 0.3 % of the total Hirshfeld surface and having $d_e + d_i \approx 2.8$ Å, are represented by two symmetrical wings on the fingerprint plot. The C-C contacts represent the overlap of aromatic ring systems, which facilitates π-π stacking,

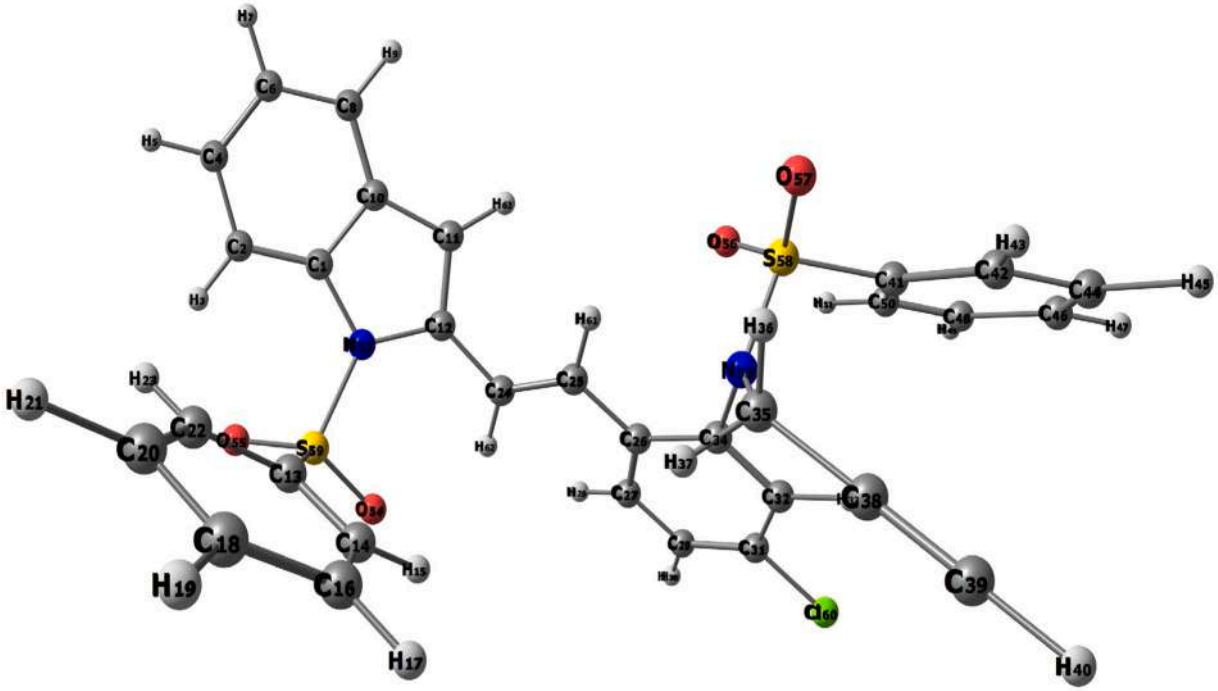

Fig. 3. Optimized structure of BS derivative.

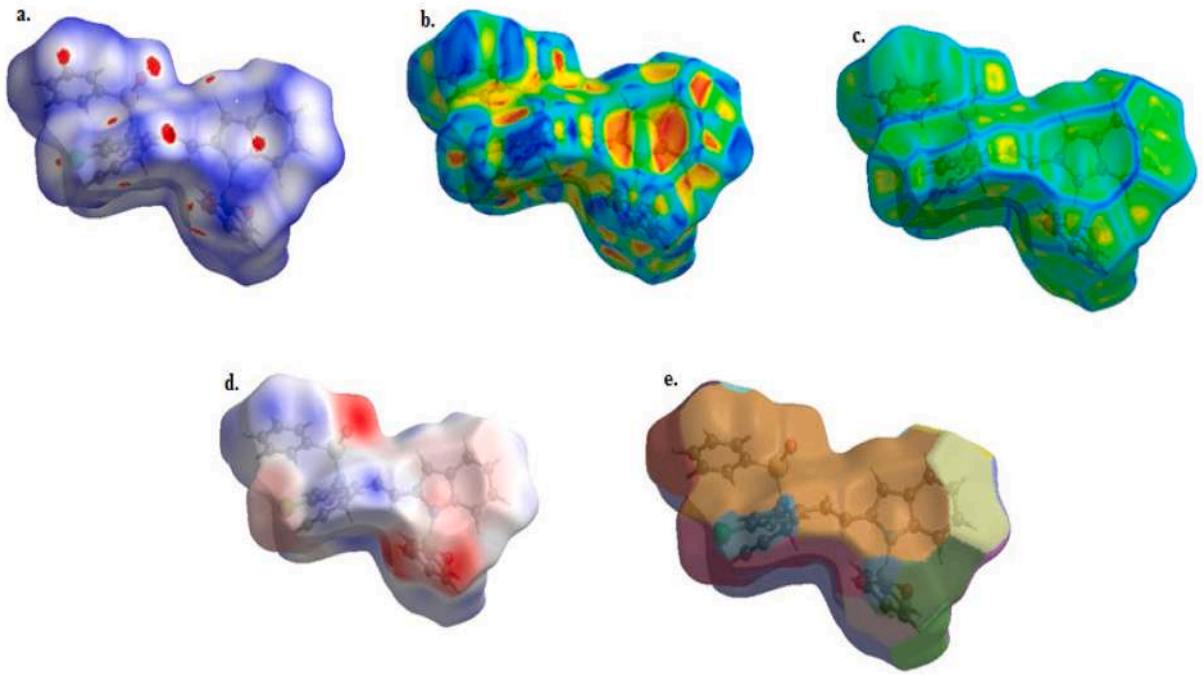

Fig. 4. View of the Hirshfeld surface of BS derivative mapped over (a) d_{norm} and (b) shape index (c) curvature (d) electrostatic potential (e) fragment patches.

a key interaction influencing molecular arrangement in the crystal lattice and established through their contribution to crystal stability. Meanwhile, the C…C contacts, associated with "π-π" stacking interactions and contributing 3.9 % to the Hirshfeld surface, appear as a distinctive triangular region around $d_e = d_i \approx 1.8$ Å [40–41]. The overall packing of the crystal structure is primarily influenced by these weak intermolecular interactions [42–43].

3.3. Molecular electrostatic potential (MEP) analysis

MEP analysis shows the distribution of electron density in molecules, helping predict their packing in crystals based on electrostatic interactions. Interactions between the regions of opposing electrostatic potential can lead to stable crystal formations, which is crucial for optimizing the material properties of BS derivatives. These compounds are known for forming hydrogen bonds and other electrostatic interactions, which are vital for their biological activity. The electrostatic

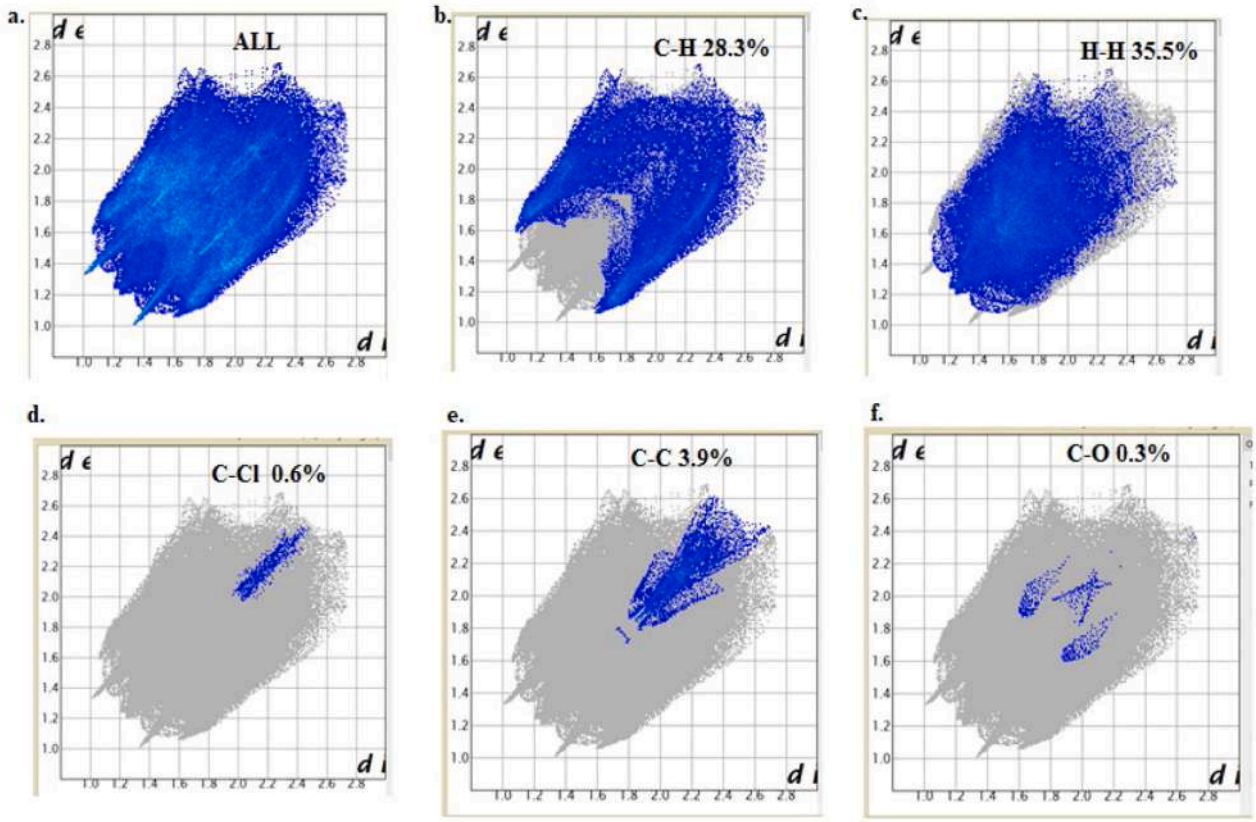

Fig. 5. Two-dimensional fingerprint plots for (a) all interactions (b) C…H/H…C (c) H…H (d) C…Cl/Cl…C (e) C…C (f) C…O/O…C.

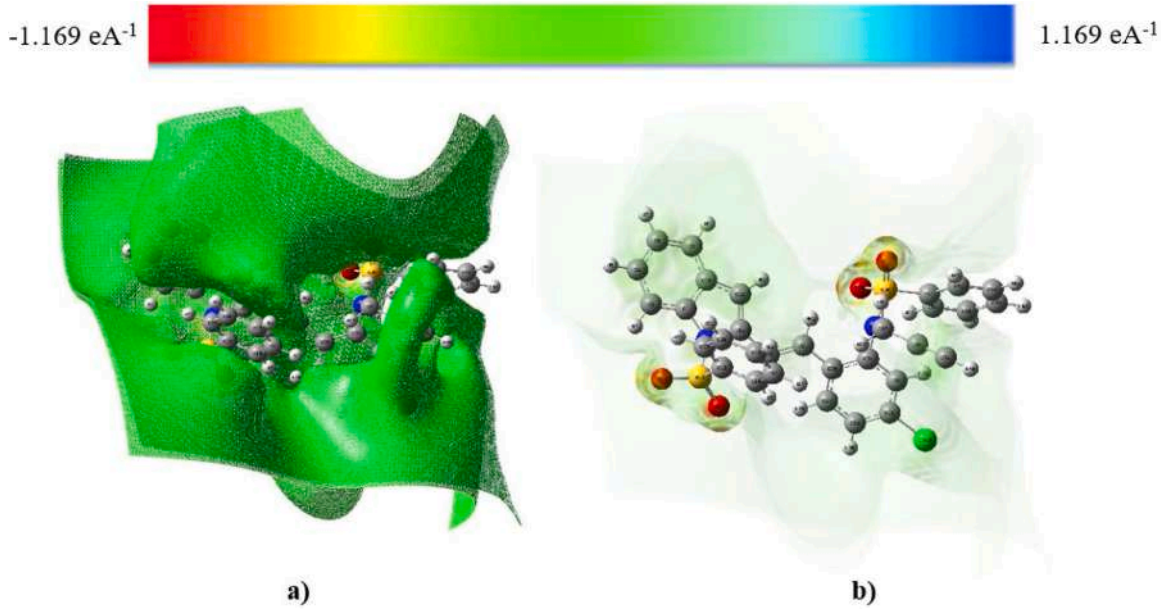

Fig. 6. a) Total electron density b) Molecular Electrostatic Potential of BS derivative.

potential V(r) is useful for identifying where nucleophilic and electrophilic reactions occur and for studying processes like molecule recognition, such as the formation of guest-host complexes in biological systems [44]. MEP represents the distribution of electric charge around a molecule, affecting its reactivity and interactions with other molecules. The presence of an electron-withdrawing atom, such as chlorine, can alter the MEP distribution. For example, a chlorine substituent can increase the positive potential on the ring, enhancing the molecule's reactivity toward nucleophiles. The interactions that lead to crystal formation are driven by changes in electron density due to chemical bonding. This redistribution of electrons is key to understanding electrostatic complementarity, which directly relates to the Molecular Electrostatic Potential (MESP). MESP shows how charges influence molecular interactions and crystal assembly. In 3D, MESP represents the

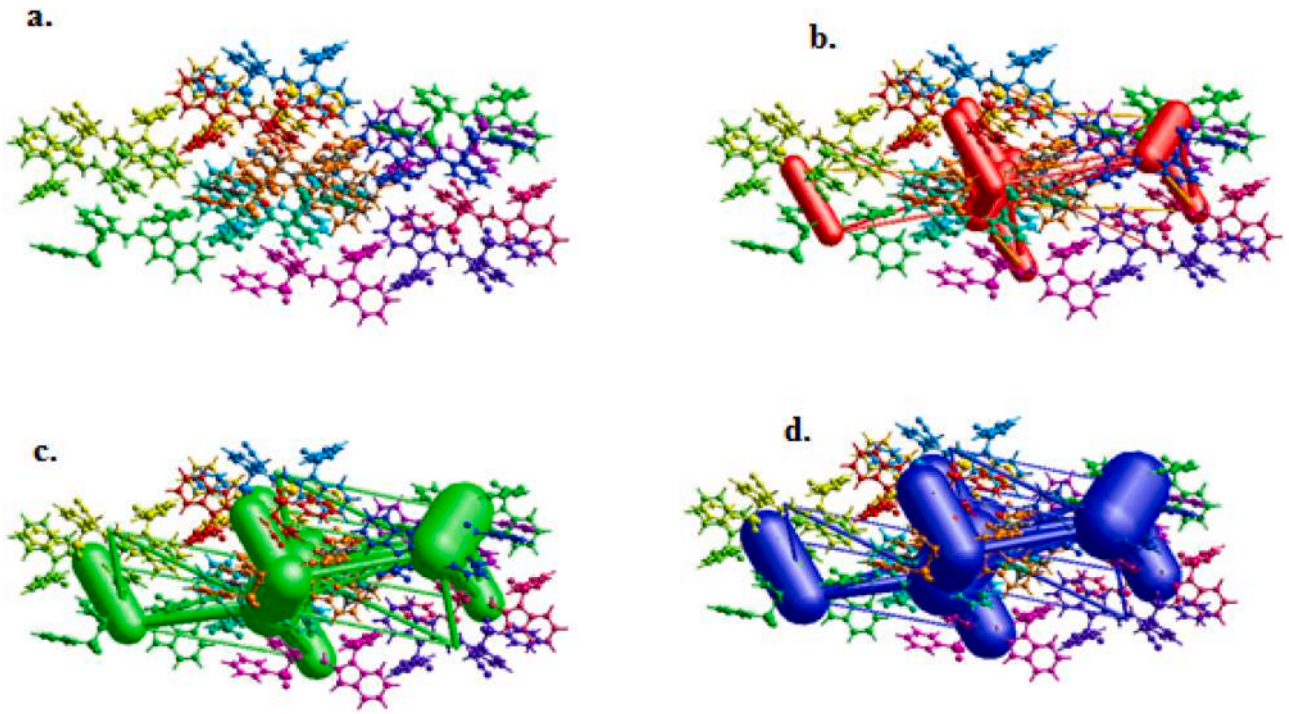

Fig. 7. (a) Interactions between the selected reference molecule (highlighted in yellow) and the molecules present in a 3.8 Å cluster around it (b) Coulomb energy framework, (c) dispersion energy framework and (d) total energy framework.

interaction between a positive charge and the overall charge distribution within a molecule, used to analyse its electrostatic properties and interactions [45]. It also helps to explain the intermolecular interactions that drive crystal nucleation and growth. The 3D electrostatic potential maps were created for each reactant and product, showing key details like size, shape, and charge density when placed over the electron density surface. These surfaces are crucial for understanding the molecular interactions and crystal formation. The different colours on the MEP surfaces represent different electrostatic potentials, with blue being the most positive and red the most negative. In the MEP structure, red indicates negative potential, and blue shows positive potential (Fig. 6).

Red regions likely indicate electronegative atoms like oxygen in the sulfonyl group (-SO_2) and nitrogen in the amide group. These red areas represent electron-rich zones, making them more likely to interact with electrophiles. The oxygen atoms in the sulfonyl group (S=O) contribute to this effect, as they often carry partial negative charges. In contrast, blue regions represent positive electrostatic potentials, typically found around hydrogen atoms attached to nitrogen (N-H) in the amide group. These electron-poor areas are more likely to interact with nucleophiles. Hydrogen atoms in the aromatic ring may also show slight positive potential, depending on their proximity to electronegative atoms.

3.4. Energy framework analysis

Energy frameworks provide a unique way to visualize the supramolecular structure of molecular crystals. By illustrating the interactions between molecules, its helps to understand how different forces, like hydrogen bonds and van der Waals forces, contribute to the crystal's overall stability and arrangement. This approach makes it easier to identify the key interactions that shape the crystal structure and design new materials with specific properties. The monomer wave functions at the HF level are used to calculate the interaction energies between the molecules of the title chemical. For a cluster of molecules with a radius of 3.8 Å surrounding the chosen molecule, the total interaction energy-which is the sum of scaled components was computed Fig. 7. The dispersion energy makes a major contribution to the interactions in the crystal, according to the energies computed using the energy model (Table 4). A cluster of molecules that were found in 2×2×2-unit cells was the subject of the energy frameworks. The dominance of the dispersion factor is further demonstrated through energy framework analysis. Positive values in the repulsion energy column (E_rep) indicate that these forces counterbalance the attractive forces to some extent. Higher repulsion energies often correlate with shorter distances between molecules. Reflects the dispersion energy, which arises from van der Waals forces. Negative values here (e.g., -10.5, -72.2, and -99.8) show attractive interactions due to dispersion forces. While electrostatic energies (E_ele) and dispersion energies (E_dis) both contribute to attraction, dispersion forces often play a more substantial role, especially in organic crystals where van der Waals forces are prominent. To detailed on the energy interactions for BS (likely referring to a specific molecular interaction or a particular type of bond or interaction site within the crystal structure) as given in Table 4.

Table 4
Interaction energies (kJmol $^{-1}$) for BS between a reference molecule and its neighbours.

N	Symop	R	E_ele	E_pol	E_dis	E_rep	E_tot
1	x, y, z	9.91	-6.4	-1.4	-10.5	2.3	-15.1
0	x, y, z	17.38	1.3	-0.7	-6.5	1.5	-3.8
0	x, y, z	16.14	-5.4	-1.5	-10.4	2.6	-13.8
0	-x, -y, -z	19.01	4.3	-0.5	-2.6	0.1	1.8
0	-x, -y, -z	7.28	-41.3	-12.1	-72.2	31.0	-89.9
0	-x, -y, -z	6.21	-49.1	-23.4	-112.2	53.5	-122.9
0	-x, -y, -z	14.45	-6.9	-3.0	-31.7	16.1	-24.4
0	x, y, z	9.16	-5.9	-4.3	-15.9	7.0	-17.5
1	-x, -y, -z	9.45	-5.2	-4.0	-30.2	17.6	-20.8
1	-x, -y, -z	6.31	-38.2	-12.8	-99.8	49.1	-97.4
1	-x, -y, -z	14.24	-2.5	-5.7	-12.7	3.8	-14.7
0	-x, -y, -z	16.70	-7.0	-1.3	-15.1	10.9	-12.8

3.5. Natural bond orbital analysis

Natural Bond Orbital (NBO) analysis is a widely used computational

Table 5
Second order perturbation theory of Fock matrix selected NBO analysis of BS.

Donor NBO (i)	Acceptor NBO (j)	E (2) kcal/mol	E(j)-E(i) a.u	F(i,j) a.u
BD(2)C13-C14	BD*(2)C20-C22	20.76	0.30	0.071
BD(2)C16-C18	BD*(2)C13-C14	24.48	0.27	0.073
BD(2)C20-C22	BD*(2)C16-C18	21.25	0.28	0.070
BD(2)C24-C25	LP*(1)C26	26.50	0.16	0.076
BD(2)C27-C29	LP*(1)C26	44.91	0.15	0.091
BD(2)C27-C29	LP(1)C31	57.72	0.11	0.091
BD(2)C32-C34	LP*(1)C26	43.70	0.16	0.092
BD(2)C32-C34	LP(1)C31	52.18	0.12	0.090
BD(2)C41-C50	BD*(2)C42-C44	20.99	0.30	0.071
BD(2)C42-C44	BD*(2)C46-C48	21.16	0.29	0.070
BD(2)C46-C48	BD*(2)C41-C50	24.23	0.27	0.073
LP(1)C31	BD*(2)C27-C29	53.88	0.18	0.105
LP(1)C31	BD*(2)C32-C34	63.04	0.17	0.108
LP(1)N52	BD*(2)C1-C10	21.55	0.34	0.080
LP(1)N52	BD*(2)C11-C12	21.72	0.35	0.078
LP(3)O54	BD*(1)N52-S59	20.50	0.40	0.082
LP(3)O55	BD*(1)N52-S59	20.75	0.39	0.082
LP(3)O56	BD*(1)O57-S58	20.07	0.57	0.097

tool in quantum chemistry, designed to provide a detailed understanding of molecular structure, bonding, and reactivity. It is particularly effective in revealing the electronic distribution within a molecule, which is crucial for predicting and explaining its chemical behaviour. NBO analysis also provides quantitative parameters, such as second-order perturbation energies, which allow for a thorough assessment of bonding interactions within a molecular system [46–48]. In this study, the NBO 3.1 module, part of the Gaussian16 software package, was used to perform the calculations. The analysis focused on determining the orbital stabilization energies (E (2)) that arise from the delocalization between donor (i) and acceptor (j) orbitals. These energies were calculated using Equation 1,

$$E_2 = \Delta E_{ij} = q_i \frac{F(i,j)2}{Ei - Ej} \quad (1)$$

Whereas, qi signifies the occupation of the donor orbital, E_i and E_j represent the energies of the donor and acceptor orbitals, respectively, and F (i, j) corresponds to the NBO Fock matrix element [49]. The NBO analysis provides valuable insights into the nature of orbital interactions, including charge transfer between donor and acceptor orbitals, which significantly contributes to the overall stabilization of the molecular system. Table 5 provides the donor-acceptor interactions in a

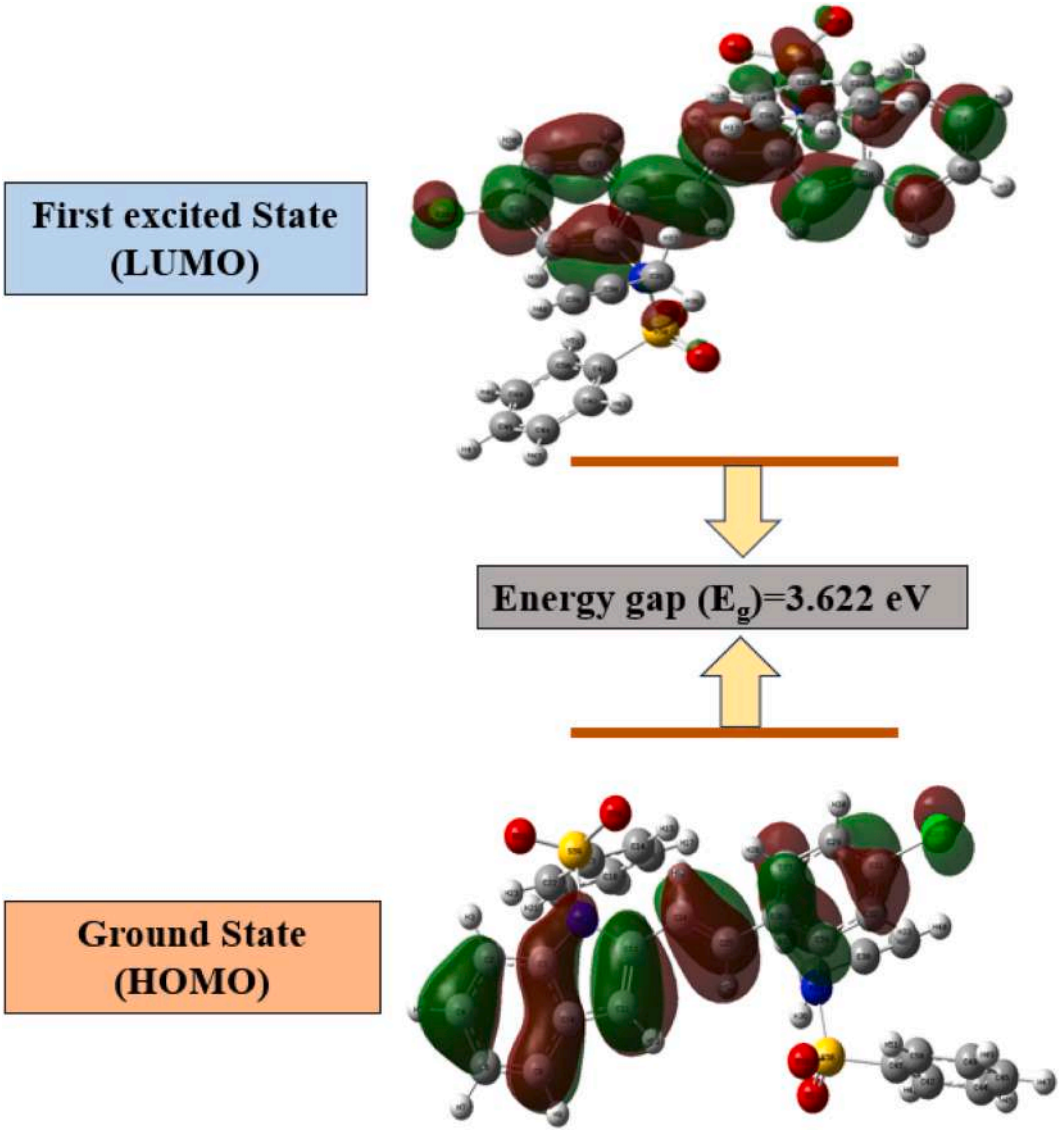

Fig. 8. HOMO-LUMO plot of BS.

Table 6
Calculated energy values of BS.

PARAMETERS	FORMULA	GAS
HOMO	E_{HOMO}	-5.58
LUMO	E_{LUMO}	-1.96
Energy gap ΔE	$-(E_{HOMO}-E_{LUMO})$	3.622
Ionization potential (A)	$-E_{HOMO}$	5.582
Electron affinity (I)	$-E_{LUMO}$	1.96
Electronegativity (χ)	(I+A)/2	3.771
Global hardness (η)	(A-I)/2	1.811
Global softness (S)	1/2η	0.906
Chemical potential (μ)	−χ	-3.77
Global electrophilicity (ω)	μ2/2η	3.926
Maximum electronic charge (ΔN_{max})	−(μ/η)	2.082

BS derivative as obtained from the B3PW91/6-31G(d,p) basis set calculation.

Lone pairs on carbon atoms can participate in resonance or conjugation, allowing for the delocalization of electron density and the formation of stabilizing interactions.

The interaction between lone pair of Carbon atom (C31) with π* (C32-C34) and π(C27-C29) has a highest stabilization energy of 63.04 and 53.88 kJmol^{-1}, respectively. The interaction between the lone pair of the nitrogen atom N52 and the π-bonding system of atoms π*(C1-C10) and π*(C11-C12) has 21.55 & 21.72 kJmol^{-1}, respectively and its lead to a stabilization of the system. This interaction could involve the donation of electron density from the lone pair to the π-system, resulting in a strengthened or delocalized bond. The bond orders indicate the extent of electron sharing and bonding between the respective carbon atom pairs.

The interaction between the bonding orbital involving carbon atoms π*(C13-C14), and the antibonding orbital involving carbon atoms π(C20-C22). The bond order associated with this interaction is 20.76 kJmol^{-1}. The interaction between the bonding orbital involving carbon atoms π(C16-C18), and the antibonding orbital involving carbon atoms π*(C13-C14).

The bond order associated with this interaction is 24.48 kJmol^{-1}. The interaction between the bonding orbital involving carbon atoms π(C20-C22), and the antibonding orbital involving carbon atoms π*(C16-C18). The bond order associated with this interaction is 21.25 kJmol^{-1}.

3.6. Frontier molecular orbital analysis

The Highest Occupied Molecular Orbital (HOMO) is the molecular orbital that contains the electrons with the highest energy in a molecule. It represents the frontier orbital from which electrons are most likely to be donated during chemical reactions. Fig. 8 shows the HOMO-LUMO (Lowest Unoccupied Molecular Orbital) plot for the BS molecule, illustrating the distribution and energy levels of these orbitals. The energy values calculated for the HOMO and LUMO, as well as their energy gap, are detailed in Table 6. This energy gap is an important parameter that influences the molecule's electronic properties, reactivity, and stability, providing insights into its behaviour in various chemical environments. Fig. 8 illustrates the Frontier Molecular Orbital plot of the BS derivative, and the calculated energy values are listed in Table 6. For the BS compound, the energy of the Highest Occupied Molecular Orbital (HOMO) is -5.58 eV, the energy of the Lowest Unoccupied Molecular Orbital (LUMO) is -1.96 eV, and the energy gap is 3.622 eV. The energy gaps of 4-Methyl-N-(3-nitrophenyl) benzene sulfonamide (1.12 eV) and 4-Methyl-N-(naphthalene-1-yl) benzene sulfonamide (4.24 eV) reflect their distinct properties [50]. The small gap (1.12 eV) indicates high reactivity and low stability, suitable for catalytic or electron-transfer applications. In contrast, the large gap (4.24 eV) suggests high stability and low reactivity, ideal for optoelectronic applications like UV-absorbing or insulating materials [51]. The present compound's moderate gap (3.622 eV) suggests a balance, making it suitable for semiconducting, UV-active, and photocatalytic applications.

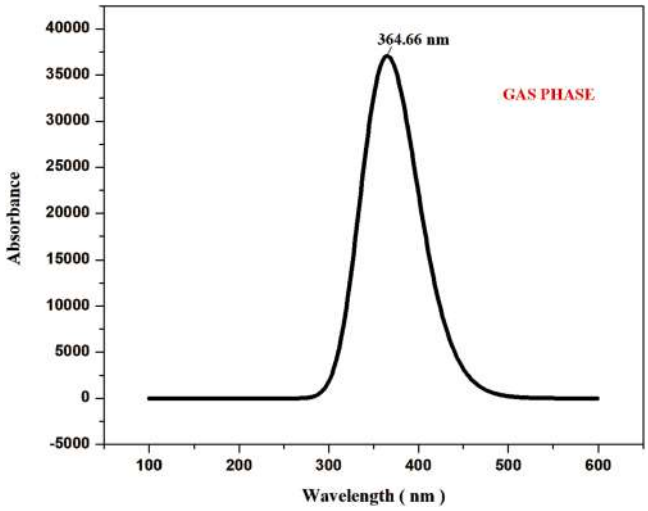

Fig. 9. TD-DFT UV-Visible spectrum of BS.

The electronegativity, chemical hardness, chemical softness, electron affinity, chemical potential, ionization potential, and electrophilicity of a molecule can be obtained by calculating its HOMO & LUMO energy values (in Table 6). The ionization potential (A) of the molecule is 5.582 eV, indicating the energy required to remove an electron, while the electron affinity (I) is 1.96 eV, reflecting the energy released upon gaining an electron. The electronegativity (χ), calculated as the average of A and I, is 3.771 eV, representing the molecule's ability to attract electrons. The global softness (S) is 0.906 eV, showing the molecule's capacity to accommodate additional electrons, which is inversely related to its global hardness (η) of 1.811 eV, a measure of its resistance to changes in electron density. The chemical potential (μ) is -3.77 eV, indicating the molecule to exchange electrons, while the global electrophilicity (ω) is 3.926 eV, suggesting its propensity to act as an electrophile. Furthermore, the maximum electronic charge (ΔN_{max}) is 2.082 eV, indicating the molecule's tendency to donate electrons.

3.7. Ultraviolet-visible analysis

UV-Visible spectroscopy is a method used to study the absorption of ultraviolet and visible light by molecules, with a spectral range from 200 to 700 nm. To analyse the molecular interactions and electronic properties of the system, time-dependent density functional theory (TD-DFT) was applied using the B3PW91/6-31G (d, p) basis set. The electrons within conjugated π systems, such as those in aromatic rings, absorb UV light and undergo a transition from bonding π orbitals to anti-bonding π* orbitals (π-π* transitions). Additionally, non-bonding electrons, such as lone pairs (LP) in functional groups like carbonyls (C=O), can absorb UV light, leading to a transition to anti-bonding π* orbitals (n-π* transitions). The absorption spectrum of the BS derivative compound shows a peak at 364.66 nm, indicating a blue shift, which can be attributed to the solvation of lone pairs (as shown in Fig. 9). This blue shift suggests that the interaction of the molecule with its environment stabilizes the lone pairs, increasing the energy gap of the n-π* transition. The energy gap of 3.622 eV implies that the material is less reactive and more chemically stable, as the transition between the highest occupied molecular orbital (HOMO) and the lowest unoccupied molecular orbital (LUMO) requires more energy. A smaller energy gap typically results in a redshift in the absorption spectrum, while a larger energy gap leads to a blue shift. In this case, the blue shift points to a relatively large energy gap, indicating strong electronic transitions. Furthermore, the transparency across the visible spectrum implies that the material could be highly suitable for optical applications, such as in transparent electronics or optoelectronic devices.

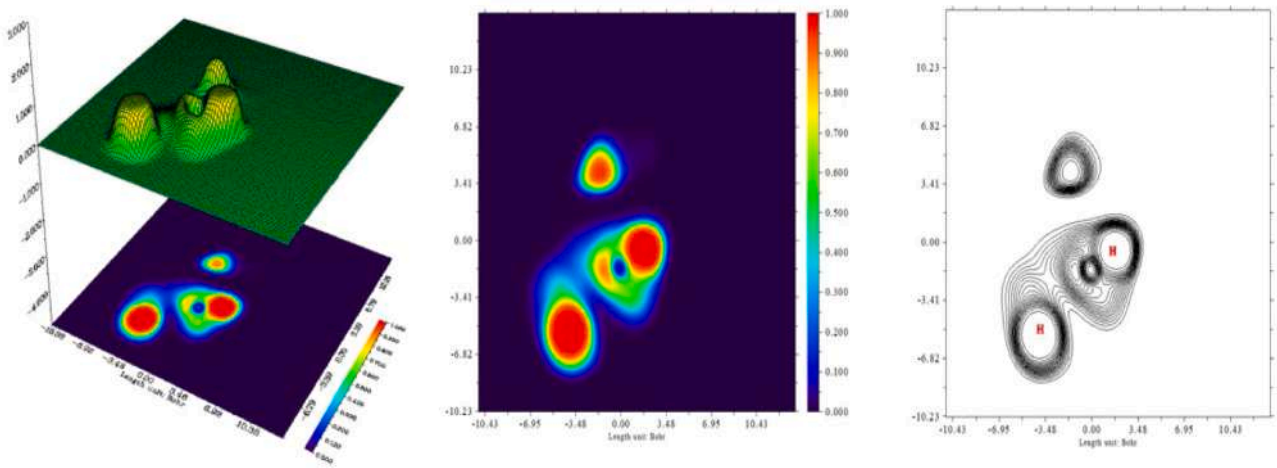

Fig. 10. a) Electron Localized Function Projection map b) Color-filled map c) Contour map of the BS derivative compound.

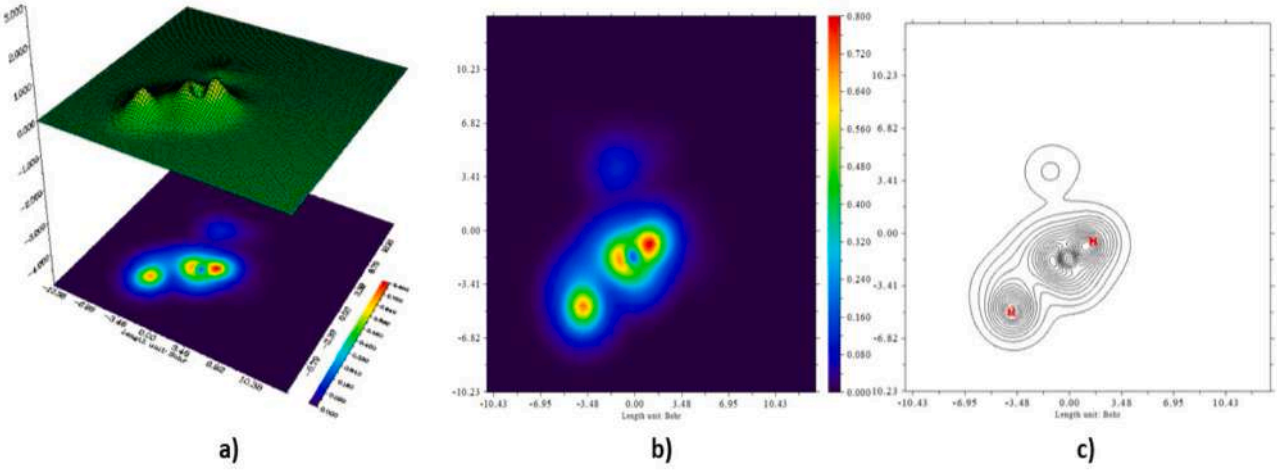

Fig. 11. a) Localized Orbital Locator Projection map b) Color-filled map c) Contour map of the BS derivative compound.

3.8. Electron localized function & localized orbital locator (ELF & LOL)

The Electron Localization Function (ELF) is a computational chemistry tool that quantifies electron localization in molecules, helping analyse chemical bonding. It distinguishes between different bonding types and identifies regions of high electron density, which are important for understanding chemical reactivity [46–47]. The Electron Localization Function (ELF) for the BS derivative provides valuable insight into the electronic structure of the compound. In this Fig. 10 regions of high electron localization, marked by red areas, likely correspond to lone pairs (LP) on electronegative atoms such as oxygen (O) in the sulfonyl group (-SO_2) & nitrogen (N) in the amide group (N-H). These regions indicate robust electron density, where the electrons are tightly bound and less available for reactivity. As well as the blue colour regions denotes the low electron localization, often found in non-bonding regions or spaces between atoms, indicating lower electron density. The ELF also highlights the delocalized electrons in the aromatic ring, where π-electrons are shared across the structure. The distribution of electron localizations used to understand the reactivity of the BS derivative compound, particularly in predicting sites for nucleophilic and electrophilic interactions, as well as its potential behaviour in crystal packing and molecular recognition processes. The Localization Orbital Locator (LOL) quantifies the extent to which an orbital is localized within a molecule or material. It provides a quantitative assessment of the electron density concentration around a specific nucleus or group of nuclei [48]. In the case of the BS derivative compound, the carbon and oxygen atoms located in the blue regions demonstrate the highest levels of Pauli repulsion. This repulsion is further evidenced by the red regions, which indicate areas where the electrons of the BS derivative compound's atoms experience the most significant Pauli repulsion (Fig. 11).

3.9. Fukui functions (FF)

The Fukui function is a widely used method in computational chemistry for predicting the reactivity of specific atoms or regions within a molecule, particularly in relation to nucleophilic and electrophilic attacks. It is used to identifies how the electron density of a molecule changes when electrons are added or removed, highlighting reactive sites. Higher values of the nucleophilic Fukui function (f^-) indicate areas most likely to accept electrons, making them susceptible to nucleophilic attack, while larger electrophilic Fukui function (f^+) values correspond to sites more prone to donating electrons, making them reactive toward electrophilic species. The Fukui function also helps predict areas vulnerable to interaction with radical species through the radical Fukui function (f^0), which highlights regions equally reactive to both nucleophiles and electrophiles. Overall, the Fukui function is a used for understanding & predicting molecular reactivity, aiding in the identification of the most reactive atoms or bonds in a molecule.

Table 7
Fukui function analysis of the bs derivative using the DFT/B3PW91/6-31G(d,p) Basis Set.

Atoms	Mulliken atomic charges			Fukui functions			Global softness			Electrophilicity		
	N(0,1)	N-1(-1,2)	N+1(1,2)	Fr+	Fr-	Fr0	sr+fr+	sr-fr-	sr0 fr0	wfr+	wfr-1	w0fr0
1C	0.282	0.268	0.314	0.032	0.014	0.046	0.029	0.013	0.041	0.179	0.05	0.163
2C	-0.121	-0.13	-0.105	0.016	0.007	0.023	0.014	0.006	0.021	0.09	0.024	0.081
3H	0.17	0.142	0.21	0.041	0.027	0.068	0.037	0.025	0.062	0.267	0.097	0.242
4C	-0.149	-0.17	-0.115	0.034	0.019	0.053	0.031	0.017	0.048	0.207	0.067	0.188
5H	0.124	0.08	0.181	0.057	0.044	0.101	0.052	0.04	0.091	0.396	0.156	0.358
6C	-0.126	-0.13	-0.122	0.004	5E-04	0.004	0.003	4E-04	0.004	0.017	0.002	0.015
7H	0.122	0.081	0.172	0.051	0.041	0.092	0.046	0.037	0.083	0.361	0.146	0.327
8C	-0.163	-0.18	-0.127	0.035	0.021	0.056	0.032	0.019	0.051	0.222	0.076	0.201
9H	0.129	0.094	0.175	0.046	0.034	0.081	0.042	0.031	0.073	0.318	0.123	0.288
10C	0.028	0.04	0.016	-0.01	-0.011	-0.023	-0.01	-0.01	-0.02	-0.09	-0.04	-0.083
11C	-0.178	-0.22	-0.129	0.049	0.041	0.091	0.045	0.037	0.082	0.355	0.147	0.322
12C	0.263	0.254	0.3	0.038	0.008	0.046	0.034	0.007	0.042	0.18	0.029	0.163
13C	-0.207	-0.21	-0.213	-0.01	0.002	-0.003	-0	0.002	-0	-0.01	0.007	-0.012
14C	-0.097	-0.1	-0.104	-0.01	0.005	-0.002	-0.01	0.004	-0	-0.01	0.016	-0.006
15H	0.171	0.168	0.167	-0	0.002	-0.001	-0	0.002	-0	-0	0.009	-0.004
16C	-0.127	-0.13	-0.124	0.003	0.002	0.005	0.003	0.001	0.004	0.018	0.006	0.017
17H	0.14	0.117	0.156	0.016	0.022	0.039	0.015	0.02	0.035	0.152	0.08	0.138
18C	-0.107	-0.12	-0.103	0.005	0.014	0.019	0.004	0.013	0.017	0.074	0.05	0.067
19H	0.139	0.105	0.164	0.024	0.034	0.058	0.022	0.031	0.053	0.229	0.121	0.207
20C	-0.123	-0.13	-0.12	0.004	0.005	0.008	0.003	0.004	0.008	0.033	0.017	0.03
21H	0.142	0.111	0.164	0.021	0.031	0.052	0.019	0.028	0.047	0.205	0.11	0.186
22C	-0.093	-0.1	-0.097	-0	0.005	0.002	-0	0.004	0.002	0.007	0.017	0.006
23H	0.167	0.152	0.169	0.001	0.015	0.017	0.001	0.014	0.015	0.066	0.055	0.06
24C	-0.148	-0.18	-0.124	0.023	0.037	0.061	0.021	0.034	0.055	0.238	0.132	0.216
25C	-0.133	-0.17	-0.087	0.046	0.037	0.084	0.042	0.034	0.076	0.328	0.133	0.297
26C	0.122	0.118	0.109	-0.01	0.003	-0.009	-0.01	0.003	-0.01	-0.03	0.012	-0.031
27C	-0.169	-0.19	-0.153	0.016	0.016	0.033	0.015	0.015	0.03	0.129	0.059	0.117
28H	0.144	0.116	0.167	0.023	0.028	0.052	0.021	0.026	0.047	0.202	0.101	0.183
29C	-0.089	-0.1	-0.081	0.008	0.008	0.015	0.007	0.007	0.014	0.06	0.027	0.054
30H	0.151	0.11	0.187	0.036	0.041	0.077	0.032	0.038	0.07	0.302	0.147	0.274
31C	-0.161	-0.19	-0.148	0.012	0.025	0.038	0.011	0.023	0.034	0.148	0.09	0.134
32C	-0.064	-0.08	-0.049	0.015	0.011	0.027	0.014	0.01	0.024	0.104	0.04	0.095
33H	0.165	0.132	0.195	0.03	0.033	0.063	0.027	0.03	0.057	0.247	0.117	0.224
34C	0.156	0.13	0.186	0.03	0.027	0.056	0.027	0.024	0.051	0.221	0.095	0.2
35C	-0.236	-0.23	-0.241	-0.01	-0.003	-0.009	-0.01	-0	-0.01	-0.04	-0.01	-0.032
36H	0.215	0.199	0.228	0.013	0.016	0.029	0.012	0.015	0.026	0.115	0.058	0.104
37H	0.182	0.189	0.174	-0.01	-0.008	-0.015	-0.01	-0.01	-0.01	-0.06	-0.03	-0.054
38C	0.277	0.295	0.263	-0.01	-0.018	-0.032	-0.01	-0.02	-0.03	-0.13	-0.06	-0.114
39C	-0.43	-0.45	-0.407	0.023	0.024	0.047	0.021	0.022	0.043	0.186	0.086	0.168
40H	0.202	0.18	0.221	0.02	0.022	0.042	0.018	0.02	0.038	0.164	0.078	0.148
41C	-0.213	-0.21	-0.218	-0	-0.005	-0.01	-0	-0	-0.01	-0.04	-0.02	-0.034
42C	-0.094	-0.1	-0.095	-0	0.002	0.002	-0	0.002	0.001	0.006	0.007	0.006
43H	0.165	0.155	0.172	0.007	0.01	0.017	0.006	0.009	0.015	0.066	0.034	0.059
44C	-0.126	-0.13	-0.124	0.002	9E-04	0.003	0.002	8E-04	0.002	0.01	0.003	0.009
45H	0.137	0.117	0.155	0.017	0.02	0.038	0.016	0.019	0.034	0.149	0.073	0.135
46C	-0.11	-0.11	-0.107	0.003	0.004	0.007	0.002	0.004	0.006	0.028	0.015	0.025
47H	0.137	0.114	0.155	0.019	0.022	0.041	0.017	0.02	0.037	0.162	0.08	0.147
48C	-0.123	-0.12	-0.122	3E-04	0.002	0.002	3E-04	0.002	0.002	0.01	0.008	0.009
49H	0.141	0.124	0.154	0.013	0.016	0.029	0.012	0.015	0.027	0.115	0.058	0.104
50C	-0.103	-0.1	-0.11	-0.01	-0.008	-0.014	-0.01	-0.01	-0.01	-0.06	-0.03	-0.051
51H	0.174	0.175	0.17	-0	-0.001	-0.005	-0	-0	-0	-0.02	-0.01	-0.019
52N	-0.779	-0.78	-0.777	0.002	0.002	0.005	0.002	0.002	0.004	0.019	0.008	0.017
53N	-0.671	-0.66	-0.681	-0.01	-0.013	-0.023	-0.01	-0.01	-0.02	-0.09	-0.04	-0.082
54O	-0.539	-0.55	-0.528	0.011	0.007	0.019	0.01	0.007	0.017	0.074	0.026	0.067
55O	-0.534	-0.56	-0.515	0.019	0.023	0.043	0.018	0.021	0.039	0.168	0.083	0.152
56O	-0.547	-0.54	-0.552	-0.01	-0.003	-0.008	-0	-0	-0.01	-0.03	-0.01	-0.028
57O	-0.551	-0.57	-0.536	0.015	0.016	0.031	0.014	0.015	0.028	0.122	0.057	0.11
58S	1.283	1.281	1.28	-0	0.003	-0.001	-0	0.002	-0	-0	0.009	-0.004
59S	1.293	1.275	1.298	0.005	0.019	0.024	0.004	0.017	0.021	0.093	0.067	0.084
60Cl	0.009	-0.07	0.101	0.091	0.081	0.172	0.083	0.073	0.156	0.676	0.288	0.613
61H	0.15	0.111	0.186	0.036	0.039	0.074	0.032	0.035	0.067	0.292	0.137	0.265
62H	0.173	0.134	0.215	0.042	0.039	0.081	0.038	0.035	0.073	0.317	0.138	0.287
63H	0.157	0.12	0.206	0.05	0.036	0.086	0.045	0.033	0.078	0.337	0.129	0.306

$$f(k^{+}) = [q(N+1) - q(N)] \quad (2)$$

$$f(k^{-}) = [q(N) - q(N-1)] \quad (3)$$

$$f(k^{0}) = 1/2[q(N+1) - q(N-1)] \quad (4)$$

whereas, f(k+): Nucleophilic attack; f(k-): Electrophilic attack; f(k0): Radial attack. In Table 7, N, N-1, and N+1 represent the Mulliken charges of the BS derivative, while q denotes the charge of an atom.

In the BS derivative under consideration, the nucleophilic attack occurs in the following ascending order as C38<N53<C26<C10<C35<C41<C22<H15<C50<C13. This sequence indicates that the carbon atom at position C13 is the most favourable site for nucleophilic attack, while C38 is the least favourable. Conversely, the order of electrophilic attack increases as follows,

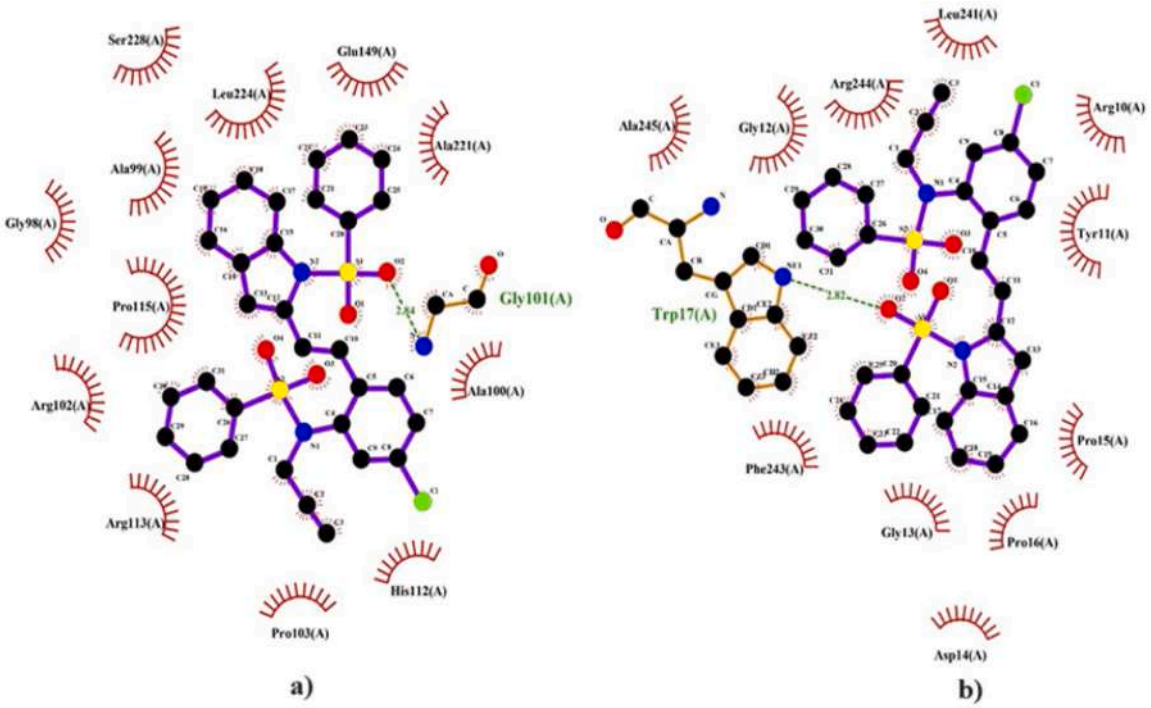

Fig. 12. **(a)** Hydrogen bond interaction of protein and ligand (First Conformer (-8.8 Kcal/mol)) **(b)** Second Conformer (-8.25 Kcal/mol).

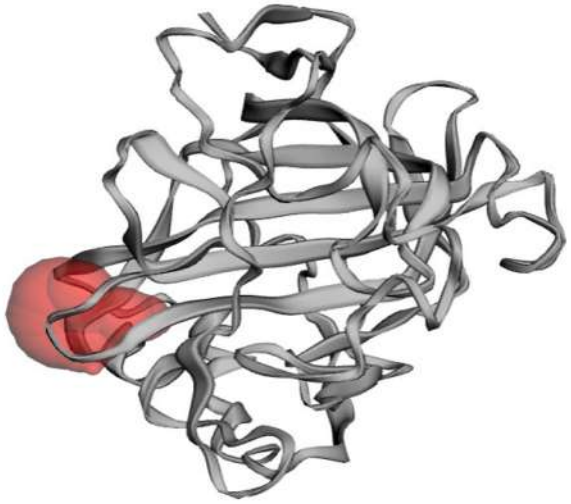

Fig. 13. Binding Site of Protein CA-9.

C42<C41<C38<C10<C4<C11<H3<H5<H7<H30. In the hydrogen atom at position H30 is the most reactive toward electrophiles, with the other sites showing progressively lower reactivity. These patterns of reactivity provide valuable insights into the mechanistic pathways that may be involved in the chemical behaviour of the derivative.

3.10. Molecular docking analysis

Molecular docking is a computational technique used to predict how small molecules, known as ligands, interact with proteins or other biomolecular targets. By simulating the binding process, docking helps to determine the optimal orientation and conformation of a ligand when it binds to a protein's active site. This technique is essential for drug discovery, helping to identify potential drug candidates and understand their binding mechanisms at the molecular level [52–53]. The Autodock vina algorithm were used for determine the interaction between the targeted protein and ligand. In this study, we employed AutoDock Tools (v 4.2.6) to analyse the interactions between the compounds. The crystal structure of Carbonic Anhydrase IX (CA-9) was retrieved from the Protein Data Bank with PDB ID: 5FL4 [54]. Excess water molecules and ligands were removed from the structure. Both the protein and the ligand need to be in pdbqt format for docking studies. Protein preparation involved adding hydrogen atoms, assigning AD4 atom types, and applying Kollman charges. The ligand, Benzene Sulphonamide (BS), was also prepared in pdbqt format. Binding cavities for CA-9 were identified using the CASTp web server [55]. AutoDock Tools were used to prepare the protein and ligand, with a grid box of 90 Å x 90 Å x 90 Å generated around the center of the ligand. The ligand binding was predicted using the Lamarckian genetic algorithm, running ten confirmations. The resulting protein-ligand complex structures and associated energies were analyzed to identify the lowest energy conformations. Ten confirmations were obtained since the number of GA runs was set to 10. Because the lower the binding energy is higher the inhibition of protein activity. From the obtained ten confirmations, two confirmations were shown to be the best binding affinity of -8.8 kcal/mol (Fig. 12a) and the second confirmation has -8.25 kcal/mol was shown (Fig. 12b). Binding Site of Protein CA-9 is shown in Fig. 13.

The interaction between the protein and ligand was observed in Ligplot+ software, which provides the 2-D graphical representation of the interaction when it is given with a complex PDB structure. It has been observed from the Fig. 12a, that the first conformer which has a binding affinity of -8.8 kcal/mol shows the interaction of the Oxygen terminal of BS interacts with Gly101 of the protein with the hydrogen bond distance of 2.84 Å. Several hydrophobic interactions of Ala100, His112, Pro103, Arg113, Arg102, Pro115, Gly98, Ala99, Leu224, Ser228, Glu149 and Ala221 has been observed. Second Confirmation (Fig. 12b) has also been taken in the interaction study, The Nitrogen terminal of Trp17 interacts with the Oxygen terminal of the ligand BS with a hydrogen bond distance of 2.82 Å. Several hydrophobic interactions of Ala245, Gly12, Arg244, Leu241, Arg10, Tyr11, Pro15, Pro16, Asp14, Gly13 and Phe243 were observed. Hydrophobic interactions are the main driving force in receptor-binding interactions.

Table 8
Molecular docking parameters of BS derivative compound with 4XE3, 3QVO, 6ZD1 and 2ZGL protein's.

Protein	Total binding energy (kcal/mol)	vdW (kcal/mol)	H-bond (kcal/mol)	Electrostatic interaction (kcal/mol)
4XE3	-104.496	-96.099	-8.397	0
3QVO	-95.24	-83.24	-12	0
6ZD1	-92.68	-88.04	-4.64	0
2ZGL	-86.51	-77.01	-9.5	0

Hydrophobic interactions may arise between molecules with more carbon atoms if the protein's non-polar amino acid side chains and the lipophilic group of the ligand are close together. The relative orientation of the molecule's lipophilic groups with respect to one another makes no difference in these interactions because they are non-directional. Because our ligand complex contains more carbon atoms than usual, we have increased the hydrophobic interaction.

In addition to that the antimicrobial activity of BS was determined by protein-ligand interactions with antibacterial and antifungal proteins: Streptomyces antibioticus (4XE3) and Shigella flexneri (3QVO) antibacterial proteins Candida tropicalis (6ZD1) and Cyclocybe aegerita (2ZGL) antifungal proteins. Structure-based drug design is aided by the potent computational method known as molecular docking [56]. The PASS prediction software is used to choose the target proteins [57–58]. In Table 8, the docking parameters are displayed. The antibacterial activity of the BS compound was tested on those bacterial strains, and these proteins were chosen as a result. PDB structures of the target proteins were acquired from the RCSB protein data bank. In Fig. 14, the interactions between the ligand BS and the targeted antimicrobial proteins are shown. The interactive line with yellow spots represents the intermolecular hydrogen bond between BS and the target proteins. The sum of hydrogen bonding, electrostatic interactions, and van der Waals interactions results in the total binding energy, and the lowest binding energy reveals the stability of the compound [54,59–61]. For the system Streptomyces antibioticus carrier protein (4XE3), which combines three interactions—van der Waals (vdW, -96.099 kcal/mol), H-bonding (-8.397 kcal/mol), and no electrostatic interaction—has the lowest overall binding energy of the four proteins at-104.496 kcal/mol. With a distance of 2.9 Å, a noticeable hydrogen bonding interaction is observed between the nitrogen atom of the amino acid ILE'357 and the SO_2 atom of BS (C-H…O). Weak interactions are important in increasing the affinity of antifungal proteins for BP, as predicted by Hirshfeld surface analysis [62–65].

4. Conclusion

The benzene sulfonamide (BS) derivative, with the formula $C_{31}H_{23}ClN_2O_4S_2$, exhibits a complex crystal structure characterized by well-defined lattice parameters and significant interactions among its molecular components. The compound's weak intermolecular interactions, highlighted by Hirshfeld surface analysis, play a critical role in its crystal packing. The blue shift in its UV-Visible absorption spectrum and insights from TD-DFT analysis indicate enhanced stability and suitability for optical applications. Additionally, the Electron Localization Function (ELF) and Localization Orbital Locator (LOL) analyses reveal important electronic properties and reactivity patterns, suggesting optimal sites for nucleophilic and electrophilic attacks. The BS derivative shows strong binding interactions in molecular docking studies with Carbonic Anhydrase IX and antimicrobial proteins, positioning it as a promising candidate for drug discovery and antimicrobial applications. The comprehensive analysis of the benzene sulfonamide (BS) derivative highlights its intricate structural, electronic, and optical properties, positioning it as a multifaceted compound with significant potential in various applications. Its robust binding interactions and marked nonlinear optical activity not only suggest efficacy in drug discovery and antimicrobial roles but also open avenues for advancements in optoelectronic technologies.

Supplementary data

Crystallographic data for the structural analysis have been deposited

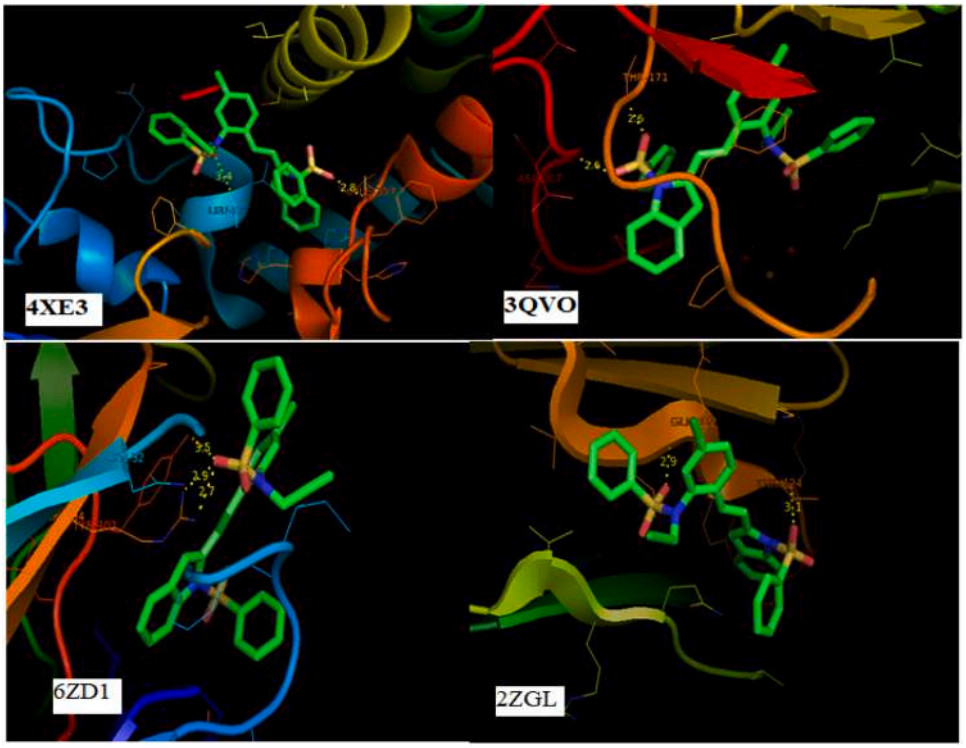

Fig. 14. Interactions of the ligand BS with the targeted antimicrobial proteins.

with the Cambridge.

Crystallographic Data Center, CCDC reference number: 2042531. Copies of this information may be obtained free of the charge,via http://www.ccd.cam.ac.uk/conts/retrieving.html or e-mail: deposit@ ccdc.cam.ac.uk.

CRediT authorship contribution statement

N. Kanagathara: Writing – review & editing, Conceptualization. **G. Dhanalakshmi:** Writing – original draft, Formal analysis, Data curation, Conceptualization. **E. Mohanapriya:** Visualization, Investigation. **Palani Manikandan:** Investigation. **A.K. Mohanakrishnan:** Writing – review & editing. **V. Sabari:** Investigation. **Dabora Vincy:** Investigation. **V. Ragavendran:** Investigation. **S. Aravindhan:** Writing – review & editing, Supervision.

Declaration of competing interest

The authors declare that they have no known competing financial interests or personal relationships that could have appeared to influence the work reported in this paper.

Supplementary materials

Supplementary material associated with this article can be found, in the online version, at doi:10.1016/j.molstruc.2025.141347.

Data availability

Data will be made available on request.

References

[1] A. Ovung, J. Bhattacharyya, Sulfonamide drugs: structure, antibacterial property, toxicity, and biophysical interactions, Bio. Phys. Rev. 13 (2) (2021) 259–272, https://doi.org/10.1007/s12551-021-00795-9.

[2] E.A. Sultan, Pathophysiologic mechanisms of immune-mediated drug hypersensitivity reactions to sulfonamides. Electronic thesis and dissertation repository, 2015, pp. 1–125. https://ir.lib.uwo.ca/etd/3430.

[3] S.M. Mathew, J. Thomas, J.T. Panicker, L.S. Kuriakose, Sulfa drugs and the skin, World J. Pharm. Res. 4 (10) (2015) 382–390.

[4] N.S. Reddy, A.S. Rao, M.A. Chari, V.R. Kumar, V. Jyothy, V. Himabindu, V. Synthesis and antibacterial activity of sulfonamide derivatives at C-8 alkyl chain of anacardic acid mixture isolated from a natural product cashew nut shell liquid (CNSL), J. Chem. Sci. 124 (2012) 723–730, https://doi.org/10.1007/s12039-012-0253-1.

[5] A. D. Pre, M. Teitler, Ro 63-0563 -a benzenesulfonamide derivative, xPharm, (2007) 1-2.https://doi.org/10.1016/B978-008055232-3.62548-6.

[6] Y. Zhao, W.R. Shadrick, M.J. Wallace, Y. Wu, E.C. Griffith, R.E.Lee J.Qi, Pterin–sulfa conjugates as dihydropteroate synthase inhibitors and antibacterial agent, Bioorg. Med. Chem. Lett 26 (16) (2016) 3950–3954, https://doi.org/10.1016/j.bmcl.2016.07.006.

[7] J.Uno A.Hanafy, H. Mitani, Y. Kang, Y. Mikami, In vitro antifungal activities of sulfa drugs against clinical isolates of Aspergillus and Cryptococcus species, Nippon Ishinkin Gakkai Zasshi 48 (1) (2007) 47–50, https://doi.org/10.3314/jjmm.48.47.

[8] A.J. Almalki, T.S. Ibrahim, E.S. Taher, M.F.A. Mohamed, M. Youns, W.A.H. Hegazy, A.M.M. Al-Mahmoudy, Synthesis, antimicrobial, anti-virulence and anticancer evaluation of new 5(4H)-oxazolone-based sulfonamides, Molecules 27 (2022) 671, https://doi.org/10.3390/molecules27030671.

[9] Y. Wan, G. Fang, H. Chen, X. Deng, Z. Tang, Sulfonamide derivatives as potential anti-cancer agents and their SARs elucidation, Eur. J. Med. Chem. 226 (2021) 113837.

[10] A. Ajeet, A.K. Mishra, Arvind Kumar, Recent advances in development of sulfonamide derivatives and their pharmacological effects- a review, Am. J. Pharmacol. Sci. 3 (1) (2015) 18–24, https://doi.org/10.12691/ajps-3-1-4.

[11] C.T. Supuran, A. Scozzafava, Carbonic anhydrase inhibitors: aromatic sulfonamides and disulfonamides act as efficient tumor growth inhibitors, J. enzyme inhibition 15 (6) (2000) 597–610, https://doi.org/10.3109/14756360009040713.

[12] G. Dhanalakshmi, V. Saravanan, A.K. Mohanakrishnan, S. Aravindhan, Crystal structures of 1-benzenesulfonyl-2-methyl-3-(4-nitrobenzoyl)-2, 3-dihydro-1H-indole and 1-benzenesulfonyl-2-methyl-3-[(thiophen-2-yl) carbonyl]-2, 3-dihydro-1H-indole, Acta Crystallogr. E 73 (10) (2017) 1555–1559, https://doi.org/10.1107/2FS2056989017012804.

[13] S. Mondal, S. Malakar, Synthesis of sulfonamide and their synthetic and therapeutic applications: recent advances, Tetrahedron 76 (48) (2020) 131662, https://doi.org/10.1016/j.tet.2020.131662.

[14] A. Scozzafava, A.Mastrolorenzo O.Takashi, C.T. Supuran, Anticancer and antiviral sulfonamides, Curr. Med. Chem. 10 (11) (2003) 925–953, https://doi.org/10.2174/0929867033457647.

[15] R.N. Mohan, S. Swamy, K.E. Manojkumar, T.MadhuChakrapani Rao, Synthesis and invitro antibacterial activity of some novel Sulfonamide derivatives bearing 1, 4-disbstituted-1, 2, 4-oxadiazole Moiety, J. Appl. Chem. 2 (4) (2013) 722–729.

[16] B.T. Gowda, R. Nayak, J. Kozisek, M. Tokarcik, H. Fuess, Benzensulfonamide, Acta. Cryst. E63 (2007) 02967, https://doi.org/10.1107/S1600536807024221.

[17] W. Xiong, M. Wei, S. Zhang Shufen, A new way to improve the light-fastness of azo reactive dyes through the introduction of benzene sulfonamide derivatives into the triazine ring, RSC Adv 9 (2019) 17658–17663, https://doi.org/10.1039/C9RA02108F.

[18] U. Ceylan, D. Mustafa, T. Hasan, Y.P. Şerife, K. Ahmet, O., 4-[(2-hydroxy-3-methylbenzylidene)amino]benzenesulfonamide, J. Mol. Struct. 1089 (2015) 222–232, https://doi.org/10.1016/j.molstruc.2015.02.042.

[19] N. Elangovan, S Sowrirajan, (E)-4-((2-hydroxy-3,5-diiodobenzylidene)amino)-N-(pyrimidine)-2-yl) benzenesulfonamide, heliyon. 7 (8) (2021) e07724, https://doi.org/10.1016/j.heliyon.2021.e07724.

[20] A. Zeenat, R. Thierry, T. Sartaj, A. Farukh, Structure elucidation {spectroscopic, single crystal X-ray diffraction and computational DFT studies} of new tailored benzenesulfonamide derived Schiff base copper (II) intercalating complexes: comprehensive biological profile {DNA binding, pBR322 DNA cleavage, topo i inhibition and cytotoxic activity, Bioorg. Chem. 94 (2020) 103427, https://doi.org/10.1016/j.bioorg.2019.103427.

[21] R.A. Mohamed-Ezzat, B.M. Kariuki, R.A. Azzam, Synthesis and crystal structure of N-(5-acetyl-4-methylpyrimidin-2-yl)benzenesulfonamide, Acta Crystallogr. E 79 (4) (2023) 331–334, https://doi.org/10.1107/S2056989023001871.

[22] CrysAlis CCD and CrysAlis Red 1.171.38.43, Rigaku Oxford Diffraction, 2015.

[23] G.M. Sheldrick, SHELXT – Integrated space-group and crystal-structure determination, Acta Cryst. A71 (2015) 3–8, https://doi.org/10.1107/S2053273314026370.

[24] G.M. Sheldrick, Crystal structure of refinement with SHELXL, Acta Cryst. C71 (2015) 3–8, https://doi.org/10.1107/S2053229614024218.

[25] M.N. Burnett, C. K. Johnson. "ORTEPIII, report ORNL-6895; Oak Ridge National Laboratory: TN, 1996.

[26] L.J. Farrugia, WinGX and ORTEP for windows: an update, J. Appl. Crystallogr. 45 (4) (2012) 849–854, https://doi.org/10.1107/S0021889812029111.

[27] C.F. Macrae, I.J. Bruno, J.A. Chisholm, P.R. Edgington, P. McCabe, E. Pidcock, P. A. Wood, Mercury CSD 2.0–new features for the visualization and investigation of crystal structures, J. Appl. Crystallogr. 41 (2) (2008) 466–470, https://doi.org/10.1107/S0021889807067908.

[28] C.F. Macrae, P.R. Edgington, P. McCabe, E. Pidcock, G.P. Shields, R. Taylor, M. Towler, S. Jacco van de, MerCURY: VISUALIZATION AND ANALYSIS OF CRYSTAL STructures, J. Appl. Cryst. 39 (2006) 453–457, https://doi.org/10.1107/S002188980600731X.

[29] M. J. Frisch, G. W. Trucks, H. B. Schlegel, G. E. Scuseria, M. A. Robb, J. R. Cheeseman, G. Scalmani, V. Barone, B. Mennucci, G. A. Petersson, H. Nakatsuji, M. Caricato, X. Li, H. P. Hratchian, A. F. Izmaylov, J. Bloino, G. Zheng, J. L. Sonnenberg, M. Hada, M. Ehara, K. Toyota, R. Fukuda, J. Hasegawa, M. Ishida, T. Nakajima, Y. Honda, O. Kitao, H. Nakai, T. Vreven, J. A. Montgomery, Jr., J. E. Peralta, F. Ogliaro, M. Bearpark, J. J. Heyd, E. Brothers, K. N. Kudin, V. N. Staroverov, T. Keith, R. Kobayashi, J. Normand, K. Raghavachari, A. Rendell, J. C. Burant, S. S. Iyengar, J. Tomasi, M. Cossi, N. Rega, J. M. Millam, M. Klene, J. E. Knox, J. B. Cross, V. Bakken, C. Adamo, J. Jaramillo, R. Gomperts, R. E. Stratmann, O. Yazyev, A. J. Austin, R. Cammi, C. Pomelli, J. W. Ochterski, R. L. Martin, K. Morokuma, V. G. Zakrzewski, G. A. Voth, P. Salvador, J. J. Dannenberg, S. Dapprich, A. D. Daniels, O. Farkas, J. B. Foresman, J. V. Ortiz, J. Cioslowski, and D. J. Fox, Gaussian, Inc., Wallingford CT, 2013. Gaussian16, Revision B.01, Gaussian, Inc., Wallingford, CT, 2016.

[30] (a) R. Ditchfield, W.J. Hehre, J.A. Pople, Self-consistent molecular-orbital methods. IX. An extended gaussian-type basis for molecular-orbital studies of organic molecules, J. Chem. Phys. 54 (1971) 724–728, https://doi.org/10.1063/1.1674902;
(b) W.J. Hehre, R. Ditchfield, J.A. Pople, Self-consistent molecular orbital methods. XII. Fur-ther extensions of gaussian-type basis sets for use in mo-lecular orbital studies of organic molecules, J. Chem. Phys. 56 (1972) 2257–2261, https://doi.org/10.1063/1.1677;
(c) </number>P.C. Hariharan, J.A. Pople, The influence of polarization functions on molecular orbital hydrogenation energies, Theor. Chim. Acta. 28 (1973) 213–222, https://doi.org/10.1007/BF00533485;
(d) </number>P.C. Hariharan, J.A. Pople, Accuracy of AH n equilibrium geometries by single determinant molecular orbital theory, Mol. Phys. 27 (1974) 209–214, https://doi.org/10.1080/00268977400100171.

[31] T. Lu, A comprehensive electron wavefunction analysis toolbox for chemists, Multiwfn, J. Chem. Phys. 161 (2024) 082503, https://doi.org/10.1063/5.0216272.

[32] S.K. Wolff, D.J. Grimwood, J.J. MacKimon, M.J. Turner, D. Jayatilaka, A.M. Spackman, Crystal explorer ver. 3.1, University of Western Australia, Perth, Australia, 2013.

[33] R.L. Beddoes, L. Dalton, J.A. Joule, O.S. Mills, J.D. Street, C.I.F. Watt, The geometry at nitrogen in N-phenylsulphonyl-pyrroles and-indoles. The geometry of sulphonamides, J. Chem. Soc., Perkin Trans. 2. (6) (1986) 787–797, https://doi.org/10.1039/P29860000787.

[34] H. Purandara, S. Foro, B.Thimme Gowda, Crystal structures of three ortho-substituted N-acylhydrazone derivatives, Acta Crystallogr., Sect. C 73 (12) (2017) 1946–1951.

[35] V.A. Bennis, A.N.E.S.S.A. V, John F. Gallagher, N—Hπ (pyrrole) Intermolecular Interactions in 1, 4-Bis (di-2-pyrrolylmethyl) benzene, Acta Crystallogr., Sect. C 54 (1) (1998) 130–132.
[36] U Chaithanya, Sabine Foro, B Thimme Gowda, N-(4-Chlorophenyl)-2-nitrobenzenesulfonamide, Acta Cryst. E. 68 (2012) o2577, https://doi.org/10.1107/S1600536812033429.
[37] B.Thimme Gowda, K.S. Babitha, M. Tokarčík, J. Kožíšek, H. Fuess, 4,6-Dimethylbenzene-1,3-disulfonamide, Acta Cryst (2007) E63, https://doi.org/10.1107/S1600536807031297, o3361.
[38] (a) A.M. Spackman, D. Jayatilaka, Hirshfeld surface analysis, Cryst. Eng. Comm 11 (2009) 19–32, https://doi.org/10.1039/B818330A;
(b) J.J. McKinnon, M.A. Spackman, A.S. Mitchell, Novel tools for visualizing and exploring intermolecular interactions in molecular crystals, Acta Cryst. B60 (2004) 627–668, https://doi.org/10.1107/S0108768104020300.
[39] J.J. McKinnon, D. Jayatilaka, M.A. Spackman, Towards quantitative analysis of intermolecular interactions with Hirshfeld surfaces, Chem. Commun. 37 (2007) 3814–3816, https://doi.org/10.1039/B704980C.
[40] A.M.D. Albert, A. Nagaraj, K. Somarathinam, P. Vinayagam, M. Arasambattu, G. Kothandan, Crystal structure and Hirshfeld surface analysis of (E)-N-(2-styrylphenyl) benzenesulfonamide, Struct. Reports 80 (2024) 10, https://doi.org/10.1107/S2056989024008892.
[41] C. Alaşalvar, N. Öztürk, A.M. Alaa, H. Gökce, A.S. El-Azab, M.A. El-Gendy, Y. Sert, Molecular structure, Hirshfeld surface analysis, spectroscopic (FT-IR, Laser-Raman, UV–vis. and NMR), HOMO-LUMO and NBO investigations on N- (12-amino-9, 10- dihydro-9, 10-ethanoanthracen-11-yl)-4- methylbenzenesulfonamide, J. Mol. Struct. 1171 (2018) 696–705, https://doi.org/10.1016/j.molstruc.2018.06.038.
[42] S. Selvaraj, P. Rajkumar, M. Kesavan, S. Gunasekaran, S. Kumaresan, R. Rajasekar, T.S. Renuga Devi, Spectroscopic and quantum chemical investigations on structural isomers of dihydroxybenzene, J. Mol. Struct. 1196 (2019) 291–305, https://doi.org/10.1016/j.molstruc.2019.06.075.
[43] M. Ashfaq, K.S. Munawar, M.N. Tahir, N. Dege, M. Yaman, S. Muhammad, M. U. Arshad, Synthesis, crystal structure, Hirshfeld surface analysis, and computational study of a novel organic salt obtained from benzylamine and an acidic component, ACS omega 6 (34) (2021) 22357–22366, https://doi.org/10.1021/acsomega.1c03078.
[44] P. Sjoberg, P. Politzer, Use of the electrostatic potential at the molecular surface to interpret and predict nucleophilic processes, J. Phys. Chem. 94 (1990) 3959–3961, https://doi.org/10.1021/j100373a017.
[45] (a)P. Politzer, D.G. Truhlar, Chemical applications of atomic and molecular electrostatic potentials, Plenum, New York, 1981. (b) </number>P. Politzer, P. R. Laurence, K. Jayasuriya, Molecular electrostatic potentials: an effective tool for the elucidation of biochemical phenomena, Environ. Health Prespect. 61 (1985) 191–202, https://doi.org/10.1289/ehp.8561191;
(c) </number>J.S. Murray, P. Politzer, The electrostatic potential: an overview, WIREs Comput. Mol. Sci. 1 (2011) 153–163, https://doi.org/10.1002/wcms.19.
[46] A. Ram Kumar, L. Ilavarasan, G. Sheeja Mol, S. Selvaraj, M. Azam, P. Jayaprakash, M. Kesavan, M. Alam, J. Dhanalakshmi, S.I. Al-Resayes, A. Ravi, Spectroscopic (FT-IR, FT-Raman, UV-Vis and NMR) and computational (DFT, MESP, NBO, NCI, LOL, ELF, RDG and QTAIM) profiling of 5-chloro-2-hydroxy-3-methoxybenzaldehyde: a promising antitumor agent, J. Mol. Struct. 1298 (2023) 136974, https://doi.org/10.1016/j.molstruc.2023.136974.
[47] A. Ram Kumar, S. Selvaraj, G.P. Sheeja Mol, M. Selvaraj, L. Ilavarasan, Sarvesh Kumar Pandey, P. Jayaprakash, Shikha Awasthi, Omeer Albormani, A. Ravi, Synthesis, solvent-solute interactions (polar and non-polar), spectroscopic insights, topological aspects, Fukui functions, molecular docking, ADME, and donor-acceptor investigations of 2-(trifluoromethyl) benzimidazole: A promising candidate for antitumor pharmacotherapy, J. Mol. Liq. 393 (2024) 123661, https://doi.org/10.1016/j.molliq.2023.123661.
[48] A.Ram Kumar, S. Selvaraj, A.S. Vickram, G.S. Mol, S. Awasthi, M. Thirunavukkarasu, M. Selvaraj, S. Basumatary, Exploring the potential of diosgenin as a promising antitumor agent through comprehensive spectroscopic characterization, solvent–solute interactions, topological properties, Hirshfeld surface, and molecular docking interactions with 2NZT and 2I1V proteins, Spectrochim. Acta A Mol. Biomol. Spectrosc. (2024) 125349, https://doi.org/10.1016/j.saa.2024.125349.
[49] N. Kanagathara, R. Usha, V. Natarajan, M.K. Marchewka, Molecular geometry, vibrational, NBO, HOMO–LUMO, first order hyper polarizability and electrostatic potential studies on anilinium hydrogen oxalate hemihydrate–an organic crystalline salt, Inorg, Nano Metal Chem 52 (2) (2022) 226–233, https://doi.org/10.1080/24701556.2021.1891103.(6).
[50] K. Sarojini, H. Krishnan, Charles C. Kanakam, S. Muthu, Synthesis, structural, spectroscopic studies, NBO analysis, NLO and HOMO–LUMO of 4-methyl-N-(3-nitrophenyl) benzene sulfonamide with experimental and theoretical approaches, Spectrochim. Acta A Mol. Biomol. Spectrosc. 108 (2013) 159–170, https://doi.org/10.1016/j.saa.2013.01.060.
[51] K. Sarojini, H. Krishnan, Charles C. Kanakam, S. Muthu, Synthesis, X-ray structural, characterization, NBO and HOMO–LUMO analysis using DFT study of 4-methyl-N-(naphthalene-1-yl) benzene sulfonamide, Spectrochim. Acta A Mol. Biomol. Spectrosc. 96 (2012) 657–667, https://doi.org/10.1016/j.saa.2012.07.037.
[52] A.Ram Kumar, S. Selvaraj, Mohammad Azam, G.P. Sheeja Mol, N. Kanagathara, Mahboob Alam, P. Jayaprakash, Spectroscopic, biological, and topological insights on lemonol as a potential anticancer agent, ACS Omega. 8 (2023) 31548–31566, https://doi.org/10.1021/acsomega.3c04922.
[53] A.Ram Kumar, L. Ilavarasan, G.P.Sheeja Mol, S. Selvaraj, Mohammad Azam, P. Jayaprakash, M. Kesavan, Mahboob Alam, J. Dhanalakshmi, Saud I. Al-Resayes, A. Ravi, Spectroscopic (FT-IR, FT-Raman, UV–Vis and NMR) and computational (DFT, MESP, NBO, NCI, LOL, ELF, RDG and QTAIM) profiling of 5chloro-2hydroxy-3-methoxybenzaldehyde: A promising antitumor agent, J.Mol. Stru. 1298 (1) (2024) 136974, https://doi.org/10.1016/j.molstruc.2023.136974.
[54] P. Gopinath, M.K. Kathiravan, Docking studies and molecular dynamics simulation of triazole benzene sulfonamide derivatives with human carbonic anhydrase IX inhibition activity, RSC Adv. 11 (60) (2021) 38079–38093, https://doi.org/10.1039/D1RA07377J.
[55] J. Dundas, Z. Ouyang, J. Tseng, A. Binkowski, Y. Turpaz, J. Liang, CASTp: computed atlas of surface topography of proteins with structural and topographical mapping of functionally annotated residues, Nucleic Acids Res 34 (2006) W116–W118, https://doi.org/10.1093/nar/gkl282. Jul 1(Web Server issue)PMID: 16844972; PMCID: PMC1538779.
[56] S.C.Palapetta S.D.Amalraj, G. Harichandran, A facile one-pot synthesis, computational and molecular docking studies of benzimidazole and benzothiazole compounds using Amberlite IRA 400-Cl resin as green/reusable catalyst, J. Mol. Struct. 1268 (2022) 133704, https://doi.org/10.1016/j.molstruc.2022.133704.
[57] D.A. Filimonov, V.V. Poroikov, Y.I. Karaicheva, R.K. Kazaryan, A.P. Budunova, Y. M. Mikhailovsky, Y.V. Burov, Computer-aided prediction of the biological activity spectrum of chemical compounds from their structural formulae: PASS systems, EKLF 58 (2) (1995) 56–62. PMID: 7773095.
[58] H.S. Mohamed, M.A. Abdelgawad, M. Hegab, Z.S. Hamza, A.M. Nagdy, S. A. Ahmed, M.M. Ghoneim, Computationl and molecular docking studies of new benzene sulfonamide drugs with anticancer and antioxidant effect, Curr.Org. Synth 20 (3) (2022) 339–350, https://doi.org/10.2174/1570179420666221007141937.
[59] R. Karthick, G. Velraj, M.P. Pachamuthu, S. Karthikeyan, Synthesis, spectroscopic, DFT, and molecular docking studies on 1, 4-dihydropyridine derivative compounds: a combined experimental and theoretical study, J. Mol. Model. 28 (2022) 1–15, https://doi.org/10.1007/s00894-021-04939-2.
[60] S. Selvakumar, M.S. Boobalan, S. Anthuvan Babu, S. Ramalingam, A. Leo Rajesh, Crystal growth and DFT insight on sodium para- nitrophenolate para- nitrophenol dihydrate single crystal for NLO applications, J. Mol. Struct. 1125 (2016) 1–11, https://doi.org/10.1016/j.molstruc.2016.05.104.
[61] M. Gümüş, S.N. Babacan, Y. Demir, Y. Sert, I. Koca, I. Gülçin, Discovery of sulfadrug–pyrrole conjugates as carbonic anhydrase and acetylcholinesterase inhibitors, Arch. Pharm. 355 (1) (2022), https://doi.org/10.1002/ardp.202100242, 2100242.
[62] A. Guesmiv, T. Roisnel, H. Marouani, Featuring non-covalent interactions in m-xylylenediaminium bis (perchlorate) monohydrate: synthesis, characterization and Hirshfeld surface analysis, J. Mol. Struct. 1194 (2019) 66–72, https://doi.org/10.1016/j.molstruc.2019.04.124.
[63] M. Medimagh, N. Issaoui, S. Gatfaoui, A.S. Kazachenko, O.M. Al-Dossary, Naveen Kumar, H. Marouani, Leda G. Bousiakoug, Investigations on the non-covalent interactions, drug-likeness, molecular docking and chemical properties of 1, 1, 4, 7, 7-pentamethyldiethylenetriammonium trinitrate by density-functional theory, J. King Saud Univ. Sci. 35 (4) (2023) 102645, https://doi.org/10.1016/j.molstruc.2019.04.124.
[64] S. Gatfaoui, H. Dhaouadi, T. Roisnel, M. Rzaigui, H. Marouani, m-Xylylenediaminium dinitrate, Acta crystallogr., E 70 (4) (2014) o398, https://doi.org/10.1107/S1600536814004620. -o399.
[65] S. Gatfaoui, H.Marouani Sofian, M. Rzaigui, 4-Methylbenzylammonium nitrate, Acta crystallogr., E 69 (9) (2013) o1453, https://doi.org/10.1107/S1600536813022836. -o1453.